

Conformal Frequency Estimation with Sketched Data under Relaxed Exchangeability

Matteo Sesia

*Department of Data Sciences and Operations
University of Southern California, Los Angeles, California, USA
sesia@marshall.usc.edu*

Stefano Favaro

*Department of Economics and Statistics
University of Torino and Collegio Carlo Alberto, Torino, Italy
stefano.favaro@unito.it*

Edgar Dobriban

*Departments of Statistics and Data Science, and of Computer and Information Science
University of Pennsylvania, Philadelphia, Pennsylvania, USA
dobriban@wharton.upenn.edu*

Abstract

A flexible method is developed to construct a confidence interval for the frequency of a queried object in a very large data set, based on a much smaller sketch of the data. The approach requires no knowledge of the data distribution or of the details of the sketching algorithm; instead, it constructs provably valid frequentist confidence intervals for random queries using a conformal inference approach. After achieving marginal coverage for random queries under the assumption of data exchangeability, the proposed method is extended to provide stronger inferences accounting for possibly heterogeneous frequencies of different random queries, redundant queries, and distribution shifts. While the presented methods are broadly applicable, this paper focuses on use cases involving the count-min sketch algorithm and a non-linear variation thereof, to facilitate comparison to prior work. In particular, the developed methods are compared empirically to frequentist and Bayesian alternatives, through simulations and experiments with data sets of SARS-CoV-2 DNA sequences and classic English literature.

Keywords: Conformal inference, distribution shift, exchangeability, sketching, uncertainty.

1. Introduction

1.1 Estimating frequency queries from sketched data

Estimating the frequency of an object given a lossy reduced representation, or *sketch*, of a big data set is a classical problem (e.g., Misra and Gries, 1982; Charikar et al., 2002, etc). This task is relevant in diverse fields including machine learning (Shi et al., 2009), cybersecurity (Schechter et al., 2010), natural language processing (Goyal et al., 2012), genetics (Zhang et al., 2014), and privacy (Cormode et al., 2018). Sketching is often practically motivated by memory limitations, as large numbers of distinct symbols may otherwise be computationally expensive to analyze (Zhang et al., 2014), or by privacy constraints, in situations where the original data contain sensitive information (Kockan et al., 2020).

There exist many sketching algorithms, several of which aim to efficiently approximate the empirical frequencies of the compressed objects. We refer to Cormode and Yi (2020) for a recent review of sketching.

Our paper studies the problem of precisely quantifying the uncertainty of empirical frequency estimates obtained from sketched data. We wish to avoid making strong assumptions about the inner workings of the sketching procedure, which may be complex and even unknown. The key ideas of the described solution are applicable regardless of how the data are compressed, but the exposition of this paper will focus for simplicity on a particularly well-known sketching algorithm and some popular variations thereof.

1.2 The count-min sketch

The count-min sketch (CMS) of Cormode and Muthukrishnan (2005) is a renowned algorithm for compressing a data set of m objects $Z_1, \dots, Z_m \in \mathcal{Z}$, belonging to a discrete and possibly infinite space \mathcal{Z} , into a representation with reduced memory footprint, while allowing approximate queries about the frequency of any $z \in \mathcal{Z}$. At the heart of the CMS lie $d \geq 1$ different w -wide hash functions $h_j : \mathcal{Z} \rightarrow [w] := \{1, \dots, w\}$, for all $j \in [d] := \{1, \dots, d\}$ and some integer number of buckets $w \geq 1$. Each hash function maps the elements of \mathcal{Z} into one of w buckets, so that distinct values of z populate the buckets approximately uniformly. Hash functions are typically chosen at random from a *pairwise independent* family \mathcal{H} . This ensures the probability (over the randomness in the choice of hash functions) that two distinct objects $z_1, z_2 \in \mathcal{Z}$ are mapped by two different hash functions into the same bucket is $1/w^2$. The data Z_1, \dots, Z_m are then compressed into a sketch matrix $C \in \mathbb{N}^{d \times w}$ with rows summing to m . The element in the j -th row and k -th column of C counts the data points mapped by the j -th hash function into the k -th bucket:

$$C_{j,k} = \sum_{i=1}^m \mathbb{1}[h_j(Z_i) = k], \quad j \in [d], k \in [w]. \quad (1)$$

One chooses d and w such that $d \cdot w \ll m$, and thus the matrix C loses information compared to the full data set; however, it has the advantage of requiring much less space to store.

Given a sketch C from (1), one may want to answer queries about the original data. For instance, one may want to estimate the empirical frequency (i.e., number of occurrences) of an object $z \in \mathcal{Z}$:

$$f_m(z) := \sum_{i=1}^m \mathbb{1}[Z_i = z]. \quad (2)$$

One solution is to return the smallest count among the d buckets into which z is mapped:

$$\hat{f}_{\text{up}}^{\text{CMS}}(z) = \min_{j \in [d]} \left\{ C_{j, h_j(z)} \right\}. \quad (3)$$

This procedure is outlined by Algorithm A5 in Appendix A. Since $\hat{f}_{\text{up}}^{\text{CMS}}(z) \geq f_m(z)$, it gives a deterministic upper bound for $f_m(z)$ (Cormode and Muthukrishnan, 2005). Although $\hat{f}_{\text{up}}^{\text{CMS}}(z)$ may be larger than $f_m(z)$ due to hash collisions, the independence of the hash functions still enables the following classical probabilistic lower bound for $f_m(z)$. Cormode

and Muthukrishnan (2005) showed that for any $\delta, \varepsilon \in (0, 1)$, choosing $d = \lceil -\log \delta \rceil$ and $w = \lceil e/\varepsilon \rceil$, for any fixed $z \in \mathcal{Z}$, and with $\hat{f}_{\text{up}}^{\text{CMS}}(z)$ from (1),

$$\mathbb{P}_{\mathcal{H}}[f_m(z) \geq \hat{f}_{\text{up}}^{\text{CMS}}(z) - \varepsilon m] \geq 1 - \delta. \quad (4)$$

For example, if $\delta = 0.05$ and thus $d = 3$, this says that $\hat{f}_{\text{up}}^{\text{CMS}}(z) - m \cdot \lceil e/w \rceil$ is a lower bound on $f_m(z)$ with 95% probability. The subscript \mathcal{H} in the bound (4) clarifies that the randomness is with respect to the hash functions, while Z_1, \dots, Z_m and z are fixed. This bound can be useful to inform the choices of d and w prior to sketching, but it is not fully satisfactory as a way of quantifying the uncertainty about the true frequency of a given query. First, it is often too conservative (Ting, 2018) if the data are randomly sampled from some distribution as opposed to being arbitrary and potentially worst-case. Second, it is not flexible: δ cannot be chosen by the practitioner because it is fixed by d , and ε is uniquely determined by the hash width. Thus, the bound (4) does not always give practical confidence intervals. As discussed below, more useful uncertainty estimates can be obtained when the data are drawn randomly.

1.3 Uncertainty estimation for sketching with random data

An alternative approach to computing lower and upper bounds for $f_m(z)$ was proposed by Ting (2018) to address the often excessive conservativeness of the classical bounds described above. The method of Ting (2018) is based on bootstrapping, and departs from classical analysis of the CMS as it leverages randomness in the data instead of randomness in the hash functions. Precisely, it assumes the data and the queried object are independent and identically distributed (i.i.d.) random samples from some unknown distribution. This condition means that one is interested in the typical behavior of the algorithm over certain scenarios described by the distribution. The condition does not always apply but, when it does, it can be extremely useful because it leads to much more informative confidence intervals. In fact, the confidence intervals described by Ting (2018) are nearly exact for the CMS, up to a finite-sample discrepancy between the bootstrap and population distributions.

A limitation of the bootstrap approach is that it relies on the specific *linear* structure of the CMS—the sketch matrix C in (3) is a linear combination of the true frequencies of all objects in the data set—and is not easily extendable to other sketching algorithms that may outperform the CMS in practice. For example, the CMS is relatively sensitive to random hash collisions, which can result in overly conservative deterministic upper bounds. This challenge has motivated the development of alternative *non-linear* algorithms, such as the CMS with *conservative updates* (CMS-CU) (Estan and Varghese, 2002). Whenever a new object z is sketched by the CMS-CU, only the row of C with the smallest value of $C_{j, h_j(z)}$ is updated, while the other counters remain unaltered. Then, a valid deterministic upper bound for the CMS-CU can be calculated with the same formula in (3). While the CMS-CU can lead to much higher query accuracy compared to the vanilla CMS (Estan and Varghese, 2002), the theoretical analysis of the CMS-CU beyond a deterministic upper bound is more challenging, and it appears to be a relatively less explored topic.

1.4 Contributions and outline

This paper develops a novel method for constructing valid and reasonably tight frequentist confidence intervals for frequency queries based on data randomly sampled from an unknown distribution and then sketched with the CMS, the CMS-CU, or any other possibly unknown sketching algorithm. Although our method requires higher computational power and memory usage compared to traditional sketching, the additional cost of our uncertainty estimates will be negligible compared to the typical size of the data sets involved.

This paper is organized as follows. Section 2 reviews relevant conformal inference background. Section 3 formally connects our problem to conformal inference and develops a method for constructing confidence intervals with exact marginal coverage for the unknown empirical frequency of a queried object. This solution assumes the data and the query are exchangeable random samples from the same unknown population, but it requires no parametric assumptions about the underlying distribution. Section 4 highlights some limitations of marginal coverage under the assumption of data exchangeability, and then it develops an alternative method which mitigates this problem by constructing confidence intervals with a stronger coverage property that holds simultaneously for rarer and more common random queries. Section 5 develops and studies a further extension of this method that accounts for all redundancies in a set of random queries and is more robust to distribution shifts. Section 6 presents applications of the developed methods to synthetic and empirical data. Section 7 concludes with a discussion and some ideas for future work.

1.5 Related work

A shorter version of this work (Sesia and Favaro, 2022) was recently accepted for publication at the NeurIPS 2022 conference. This longer manuscript contains novel methods and theoretical results (Section 5) studying the construction of confidence intervals with guaranteed coverage for a sufficiently large fraction of unique queries in a possibly redundant test set. These advances make it possible to relax the stricter query exchangeability assumptions of Sesia and Favaro (2022), expanding the practical relevance of conformalized sketching to a broader range of applications. This manuscript also contains additional simulations accompanying its novel methodological and theoretical contributions.

This work builds upon conformal inference, which was pioneered by Vovk and collaborators (Saunders et al., 1999; Vovk et al., 2005) and brought to the statistics spotlight by works such as Lei et al. (2013); Lei and Wasserman (2014); Lei et al. (2018). Although primarily conceived for supervised prediction (Vovk et al., 2009; Vovk, 2015; Lei and Wasserman, 2014; Romano et al., 2019; Izbicki et al., 2019; Park et al., 2021; Qiu et al., 2022), conformal inference has found other applications including outlier and anomaly detection (Bates et al., 2021; Kaur et al., 2022; Li et al., 2022), causal inference (Lei et al., 2021, e.g.), and survival analysis (Candès et al., 2021). We mention here that the ideas in conformal prediction have deep roots in statistics, dating back at least to the pioneering works of Wilks (1941), Wald (1943), Scheffe and Tukey (1945), and Tukey (1947, 1948); see also Geisser (2017).

To the best of our knowledge, the potential of conformal inference for use in sketching remained untapped before Sesia and Favaro (2022). There exist many algorithms for using sketches to compute approximate frequency queries; some are similar to the CMS (Fan et al., 2000; Goyal and Daumé, 2011; Pitel and Fouquier, 2015; Cormode and Yi, 2020),

while others may involve complex learning algorithms (Hsu et al., 2019; Jiang et al., 2019). Our approach is applicable to all of them, but here we focus more on the CMS because it provides a familiar example that facilitates the exposition. As we will make use of conformal inference, a brief review of the relevant background is provided in the next section. More general forms of randomized sketching have also been studied for other numerical, statistical, and learning problems (Vempala, 2005; Halko et al., 2011; Mahoney, 2011; Woodruff, 2014; Drineas and Mahoney, 2016; Martinsson and Tropp, 2020), see e.g., Dobriban and Liu (2019); Liu and Dobriban (2019); Lacotte and Pilanci (2020); Yang et al. (2021).

Various confidence bounds have been developed for the CMS (Cormode and Yi, 2020), most of them treating the data as fixed and only using the hashing randomness, similarly to the bound (4). More recently, uncertainty estimation for the CMS based on data randomness has been studied by Ting (2018) from a frequentist perspective, as mentioned in Section 1.3, and by Cai et al. (2018) and Dolera et al. (2021) from a Bayesian perspective. More precisely, Cai et al. (2018) and Dolera et al. (2021) model the data with a prior distribution and compute the posterior of the queried frequencies given the sketch. Our work is closer to Ting (2018) in that we treat the data as random while seeking frequentist probabilistic guarantees. However, our approach is very different from that of Ting (2018): the latter exploits the specific linear structure of the CMS, while we view the sketch as a black box and use conformal inference to obtain exact finite-sample inferences.

2. Preliminaries on conformal prediction

Consider *supervised learning*, in which the data samples are pairs (X_i, Y_i) , where X_i are a vector of *features* for the i -th observation and Y_i are the corresponding *outcome* or *label*; Y_i can be continuous- or discrete-valued. The goal is to use the information in $(X_1, Y_1), \dots, (X_m, Y_m)$ to learn a mapping between features and labels that enables accurate predictions of the unseen label Y_{m+1} of a new sample with features X_{m+1} . In particular, conformal prediction can be used to construct a prediction interval $[\hat{L}_{m,\alpha}(X_{m+1}), \hat{U}_{m,\alpha}(X_{m+1})]$ with guaranteed *marginal coverage*:

$$\mathbb{P}[\hat{L}_{m,\alpha}(X_{m+1}) \leq Y_{m+1} \leq \hat{U}_{m,\alpha}(X_{m+1})] \geq 1 - \alpha, \quad (5)$$

for any fixed $\alpha \in (0, 1)$, assuming that $(X_1, Y_1), \dots, (X_{m+1}, Y_{m+1})$ are exchangeable random samples from some unknown distribution over (X, Y) . Conformal prediction is flexible, as it can leverage any machine learning algorithm to approximately reconstruct the relation between X and Y , capturing it in $\hat{L}_{m,\alpha}, \hat{U}_{m,\alpha}$. This can yield relatively short intervals satisfying (5). Note that, while it is sufficient to focus on conformal intervals in this paper, similar techniques can also be used to construct more general prediction sets (e.g., Vovk et al., 2005; Romano et al., 2020b; Angelopoulos et al., 2021, etc).

A simple version of conformal prediction—known as split or inductive conformal prediction (Papadopoulos et al., 2002; Lei et al., 2018)—begins by randomly splitting the observations into two disjoint subsets, assumed for simplicity to have equal size $n = m/2$. The first n samples are spent to fit a black-box machine learning model for predicting Y given X ; e.g., a neural network or a random forest. The out-of-sample predictive accuracy of this model is then measured in terms of a *conformity score* for each of the n held-out data points. In combination with the model learnt from the first half of the data, the quantiles

of the empirical distribution of these scores are used to construct prediction intervals for future test points as a function of X_{m+1} . These intervals are guaranteed to cover Y_{n+1} with probability at least $1 - \alpha$, treating all data as random. The details of this procedure will be clarified shortly. Importantly, the coverage holds in finite samples, regardless of the accuracy of the machine learning model, as long as X_{m+1} is exchangeable with the n held-out data points. It is unnecessary for the training data to be also exchangeable, as these may be viewed as fixed.

The implementation of conformal inference depends on the choice of conformity scores. An intuitive explanation imagines that from the fitted machine learning model one constructs for each x a *nested sequence* (Vovk et al., 2005; Gupta et al., 2022) of prediction intervals $[\hat{L}_{m,\alpha}(x;t), \hat{U}_{m,\alpha}(x;t)]$, indexed by $t \in \mathcal{T} \subseteq \mathbb{R}$. This sequence is nested, in the sense that $\hat{L}_{m,\alpha}(x;t_2) \leq \hat{L}_{m,\alpha}(x;t_1)$ and $\hat{U}_{m,\alpha}(x;t_2) \geq \hat{U}_{m,\alpha}(x;t_1)$ for all $t_2 \geq t_1$. Further, assume there exists $t_\infty \in \mathcal{T}$ such that $\hat{L}_{m,\alpha}(x;t_\infty) \leq Y \leq \hat{U}_{m,\alpha}(x;t_\infty)$ almost surely for all x . For example, one may consider the sequences $\hat{\psi}_m(x) \pm t$, $t \geq 0$, where $\hat{\psi}_m$ is a regression function for a bounded label Y given X learnt by the black-box machine learning model and t plays the role of a predictive standard error.

Then, the conformity score for a data point with features $X = x$ and label $Y = y$ is defined as the smallest index t such that y is contained in the sequence of prediction intervals corresponding to x :

$$E(x, y) := \inf \{t \in \mathcal{T} : Y \in [\hat{L}_{m,\alpha}(x;t), \hat{U}_{m,\alpha}(x;t)]\}. \quad (6)$$

Let $\mathcal{I}^{\text{calib}} \subset \{1, \dots, m\}$ be the subset of held-out data points, assumed without loss of generality to have cardinality $n = m/2$. Let $\hat{Q}_{n,1-\alpha}$ be the $\lceil (1 - \alpha)(n + 1) \rceil$ smallest conformity score $E(X_i, Y_i)$ among all $i \in \mathcal{I}^{\text{calib}}$. The conformal prediction interval for a new data point with features X_{m+1} is:

$$[\hat{L}_{m,\alpha}(X_{m+1}; \hat{Q}_{n,1-\alpha}), \hat{U}_{m,\alpha}(X_{m+1}; \hat{Q}_{n,1-\alpha})]. \quad (7)$$

Intuitively, this satisfies (5) because Y_{m+1} falls outside (7) if and only if $E(X_{m+1}, Y_{m+1}) > \hat{Q}_{n,1-\alpha}$. The rest of the proof is a simple exchangeability argument; see Vovk et al. (2005), Romano et al. (2019), or the proof of Theorem 1 in Appendix C.

3. Confidence intervals with marginal coverage

3.1 Data exchangeability and conformal confidence intervals

In this section, we assume that the m data points to be sketched, Z_1, \dots, Z_m , are exchangeable random samples from some distribution P_Z on \mathcal{Z} . Some limitations of this assumption will be addressed later in Sections 4 and 5. For now, we simply emphasize that exchangeability is more restrictive compared to the classical setting reviewed in Section 1.2, which treats the data as fixed and thus can also handle non-stationary streams or adversarial cases, but it is not always unrealistic. For example, it may be justified for applications in which objects from a large data set are processed in a random order; see Sections 6 and 7 for further details. Imagining the data as approximately i.i.d. samples from some distribution is an idea that has been suggested before in the context of sketching (Ting, 2018; Cai et al., 2018; Dolera et al., 2021). However, our perspective involves three key novelties: first,

we do not assume independence; second, we allow the common distribution P_Z to remain completely unknown; and, third, we take a completely agnostic view of the inner workings of the sketching algorithm, as explained next.

Consider an arbitrary *sketching* function $\phi : \mathcal{Z}^m \rightarrow \mathcal{C}$, where \mathcal{C} is a space of dimensions lower than \mathcal{Z}^m . For example, ϕ may represent the CMS or CMS-CU methods, in which case $\mathcal{C} = \mathbb{N}^{d \times w}$, for some d, w . In general, we will treat ϕ as a *black box* and allow it to be anything, possibly involving randomization such as random hashing. The goal is to leverage the exchangeability of the data and the information in $\phi(Z_1, \dots, Z_m)$ to estimate the unobserved empirical frequency $f_m(z)$ of an object $z \in \mathcal{Z}$, defined as in (2), while accounting for uncertainty. More precisely, although still informally speaking, we would like to construct a *confidence interval* $[\hat{L}_{m,\alpha}(z), \hat{U}_{m,\alpha}(z)]$ guaranteed to contain $f_m(z)$ “with probability at least $1 - \alpha$ ”, where the randomness is with respect to the data sampling.

One way to address the above problem is to imagine the query z is also randomly sampled exchangeably with Z_1, \dots, Z_m . This is a convenient but quite strong assumption that will be partly relaxed later in Sections 4–5. With this premise, we refer to z as Z_{m+1} and focus on computing a confidence interval¹ $[\hat{L}_{m,\alpha}(Z_{m+1}), \hat{U}_{m,\alpha}(Z_{m+1})]$ depending on $\phi(Z_1, \dots, Z_m)$ that is reasonably short and guarantees marginal coverage of f_m from (2):

$$\mathbb{P}[\hat{L}_{m,\alpha}(Z_{m+1}) \leq f_m(Z_{m+1}) \leq \hat{U}_{m,\alpha}(Z_{m+1})] \geq 1 - \alpha. \quad (8)$$

Above, the probability is with respect to the data in Z_1, \dots, Z_m as well as to the randomness in the query Z_{m+1} . The interpretation of (8) is as follows: the confidence interval will cover $f_m(Z)$ for at least fraction $1 - \alpha$ of all future test points Z , if the queries and the sketched objects are sampled exchangeably from the same data generating model. Below, we will develop a method to construct reasonably tight confidence intervals satisfying (8).

3.2 Conformalization methodology

In the attempt to adapt conformal inference to address the sketching problem defined above, the first difficulty is that our task concerns data recovery, not supervised prediction. We propose to overcome this challenge by storing the true frequencies for all objects in the first m_0 observations, with $m_0 \ll m$ but sufficiently large subject to memory constraints. Without loss of generality, assume $m_0 \ll m$; otherwise, the problem becomes trivially easy. Let $n \leq m_0$ indicate the number of distinct objects among the first m_0 observations. The memory required to store these frequencies is $O(n)$, which will typically be negligible as long as m_0 is also small compared to the size $|\mathcal{C}|$ of the sketch. This approach turns our task into supervised prediction, as detailed below.

During an initial *warm-up* phase, the frequencies (or, counts) of the n distinct objects among the first m_0 observations from the data stream, Z_1, \dots, Z_{m_0} , are stored exactly into f_{m_0} , defined for all $z \in \mathcal{Z}$ as

$$f_{m_0}^{\text{wu}}(z) := \sum_{i=1}^{m_0} \mathbb{1}[Z_i = z]. \quad (9)$$

1. Since $f_m(Z_{m+1})$ is also random, it is technically speaking a prediction interval, not a confidence interval. However, we still refer to it as a confidence interval to keep the terminology consistent with prior work.

Next, the remaining $m - m_0$ data points are streamed and sketched, storing also the true frequencies for all instances of objects already seen during the warm-up phase. In other words, the following counters are computed and stored along with the sketch $\phi(Z_{m_0+1}, \dots, Z_m)$:

$$f_{m-m_0}^{\text{sv}}(z) := \begin{cases} \sum_{i=m_0+1}^m \mathbb{1}[Z_i = z], & \text{if } f_{m_0}^{\text{wu}}(z) > 0, \\ 0, & \text{otherwise.} \end{cases} \quad (10)$$

Again, this requires only $O(n)$ memory. Now, let us define the variable Y_i for all $i \in \{1, \dots, m_0\} \cup \{m+1\}$ as the true frequency of Z_i among Z_{m_0+1}, \dots, Z_m :

$$Y_i := \sum_{i'=m_0+1}^m \mathbb{1}[Z_{i'} = Z_i]. \quad (11)$$

Note that Y_i is observable for $i \in \{1, \dots, m_0\}$, in which case $Y_i = f_{m-m_0}^{\text{sv}}(Z_i)$. For a new query, Z_{m+1} is the target of inference—in truth, the ultimate target is $f_m(Z_i) = Y_i + f_{m_0}^{\text{wu}}(Z_i)$, but the second term is already known exactly. To complete the connection to supervised prediction, one still needs to define meaningful features X , and this is where the sketch $\phi(Z_{m_0+1}, \dots, Z_m)$ comes into play. For each $i \in \{1, \dots, m_0\} \cup \{m+1\}$, define X_i as the vector containing the query and the information in the sketch:

$$X_i := (Z_i, \phi(Z_{m_0+1}, \dots, Z_m)). \quad (12)$$

Then, it can be shown that the pairs $(X_1, Y_1), \dots, (X_{m_0}, Y_{m_0}), (X_{m+1}, Y_{m+1})$ are exchangeable with one another. Note that all mathematical proofs are in Appendix C.

Proposition 1 *If the data Z_1, \dots, Z_{m+1} are exchangeable, the pairs of random variables $(X_1, Y_1), \dots, (X_{m_0}, Y_{m_0}), (X_{m+1}, Y_{m+1})$ in (11)–(12) are exchangeable with one another.*

The result in Proposition 1 opens the door to applying conformal inference to the supervised observations $(X_1, Y_1), \dots, (X_{m_0}, Y_{m_0})$ in order to predict Y_{m+1} given X_{m+1} , guaranteeing marginal coverage. In particular, one can randomly split the observations indexed by $\{1, \dots, m_0\}$ into a training subset, namely $\{1, \dots, m_0^{\text{train}}\}$ for some fixed $m_0^{\text{train}} < m_0$, and a disjoint calibration subset, namely $\{m_0^{\text{train}} + 1, \dots, m_0\}$. The observations indexed by $\{1, \dots, m_0^{\text{train}}\}$ are used for fitting a data-driven predictor for computing nested confidence intervals, $[\hat{L}_{m,\alpha}(\cdot; t), \hat{U}_{m,\alpha}(\cdot; t)]$, $t \in \mathcal{T}$; see the next section for further implementation details. The observations indexed by $\{m_0^{\text{train}} + 1, \dots, m_0\}$ are used to compute conformity scores and calibrate a suitable value for the parameter t which can guarantee valid marginal coverage for a new test query in finite samples, following the general approach reviewed in Section 2. This solution is outlined step-by-step in Algorithms 1–2. Note that Algorithm 2 outputs the final confidence interval after Algorithm 1 sketches and pre-processes the data. This modular organization will prove useful in the following sections to simplify the exposition of extensions of our methodology. The following result states that the confidence interval output by Algorithm 2 has the desired marginal coverage.

Theorem 1 *If the data Z_1, \dots, Z_{m+1} are exchangeable, the confidence interval output by Algorithm 2 satisfies the marginal coverage property defined in (8).*

Algorithm 1 Conformalized sketching (data sketching, training, and calibration)

Input: Data set Z_1, \dots, Z_m . Sketching function ϕ . Warm-up period $m_0 \ll m$.
A (trainable) predictor to compute nested intervals $[\hat{L}_{m,\alpha}(\cdot; t), \hat{U}_{m,\alpha}(\cdot; t)]_{t \in \mathcal{T}}$.
Number of data points $m_0^{\text{train}} < m_0$ used for training $[\hat{L}_{m,\alpha}(\cdot; t), \hat{U}_{m,\alpha}(\cdot; t)]$.
Initialize a sparse dictionary $f_{m_0}^{\text{wu}}(z) = 0, \forall z \in \mathcal{Z}$.
for $i = 1, \dots, m_0$ **do**
 Increment $f_{m_0}^{\text{wu}}(Z_i) \leftarrow f_{m_0}^{\text{wu}}(Z_i) + 1$.
Initialize a sparse dictionary $f_{m-m_0}^{\text{sv}}(z) = 0, \forall z \in \mathcal{Z}$.
Initialize an empty sketch $\phi(\emptyset)$.
for $i = m_0 + 1, \dots, m$ **do**
 Update the sketch ϕ with the new observation Z_i .
 if $f_{m_0}^{\text{wu}}(Z_i) > 0$ **then**
 Increment $f_{m-m_0}^{\text{sv}}(Z_i) \leftarrow f_{m-m_0}^{\text{sv}} + 1$.
for $i = 1, \dots, m_0$ **do**
 Set $X_i = (Z_i, \phi(Z_{m_0+1}, \dots, Z_m))$ as in (12).
 Set $Y_i = f_{m-m_0}^{\text{sv}}(Z_i)$.
Train $[\hat{L}_{m,\alpha}(\cdot; t), \hat{U}_{m,\alpha}(\cdot; t)]$ using the data in $\{(X_i, Y_i)\}_{i=1}^{m_0^{\text{train}}}$.
for $i = m_0^{\text{train}} + 1, \dots, m_0$ **do**
 Compute the conformity score $E(X_i, Y_i)$ with (6), using $[\hat{L}_{m,\alpha}(\cdot; t), \hat{U}_{m,\alpha}(\cdot; t)]$.
Output: Data sketch ϕ ;
 Sparse frequency dictionary $f_{m_0}^{\text{wu}}(z), \forall z \in \mathcal{Z}$;
 Trained predictor $[\hat{L}_{m,\alpha}(\cdot; t), \hat{U}_{m,\alpha}(\cdot; t)]$;
 Conformity scores $E(X_i, Y_i)$ for all $i \in \{m_0^{\text{train}} + 1, \dots, m_0\}$.

Algorithm 2 Conformalized sketching with marginal coverage

Input: Same as for Algorithm 1.
Random query Z_{m+1} . Desired coverage level $1 - \alpha \in (0, 1)$.
Compute using Algorithm 1:
 Data sketch ϕ ; a sparse frequency dictionary $f_{m_0}^{\text{wu}}(z), \forall z \in \mathcal{Z}$;
 Variables $X_i = (Z_i, \phi(Z_{m_0+1}, \dots, Z_m))$ and $Y_i = f_{m-m_0}^{\text{sv}}(Z_i)$ for $i \in \{1, \dots, m_0\}$.
 Trained predictor for computing nested intervals $[\hat{L}_{m,\alpha}(\cdot; t), \hat{U}_{m,\alpha}(\cdot; t)]_{t \in \mathcal{T}}$;
 Conformity scores $E(X_i, Y_i)$ for all $i \in \{m_0^{\text{train}} + 1, \dots, m_0\}$.
Compute $\hat{Q}_{n_0, 1-\alpha}$ as the $\lceil (1 - \alpha)(n_0 + 1) \rceil$ smallest score, with $n_0 = m_0 - m_0^{\text{train}}$.
Set $X_{m+1} = (Z_{m+1}, \phi(Z_{m_0+1}, \dots, Z_m))$ as in (12).
Output: a $(1 - \alpha)$ -level confidence interval

$$\left[f_{m_0}^{\text{wu}}(Z_{m+1}) + \hat{L}_{m,\alpha}(X_{m+1}; \hat{Q}_{n_0, 1-\alpha}^*), f_{m_0}^{\text{wu}}(Z_{m+1}) + \hat{U}_{m,\alpha}(X_{m+1}; \hat{Q}_{n_0, 1-\alpha}^*) \right]$$

for the unobserved frequency $f_m(Z_{m+1})$ of Z_{m+1} defined in (2).

Remark. Algorithm 2 could be trivially modified to output perfect “singleton” confidence intervals for any new queries that happen to be identical to an object previously observed during the warm-up phase. We will not take advantage of this option in the ex-

periments presented in this paper in order to provide a fairer comparison with alternative methods which do not involve a similar warm-up phase.

3.3 Conformity scores for one-sided confidence intervals

In principle, Algorithms 1–2 can accommodate any data-adaptive predictor for computing nested confidence intervals, which may depend on Z_{m+1} and on the sketch $\phi := \phi(Z_{m_0+1}, \dots, Z_m)$. Two concrete options are described here. For simplicity, we focus on one-sided confidence intervals; that is, we seek a lower bound for $f_m(X_{m+1})$. This is useful when a deterministic upper bound $\hat{f}_{\text{up}}(Z_{m+1}) \geq f_m(Z_{m+1})$ is already available, as it is the case with the CMS or CMS-CU. In such cases, one can simply set $\hat{U}_{m,\alpha}((z, \phi); t) := \hat{f}_{\text{up}}(z)$ and focus on computing $\hat{L}_{m,\alpha}(\cdot; t)$. The construction of two-sided confidence intervals is explained in Appendix A.3 in the interest of space.

To construct the lower bound $\hat{L}_{m,\alpha}(\cdot; t)$ of a one-sided interval, perhaps the simplest option is to use a fixed rule such as:

$$\hat{L}_{m,\alpha}^{\text{fixed}}((z, \phi); t) := \max\{0, \hat{f}_{\text{up}}(Z_{m+1}) - t\}, \quad t \in \{0, 1, \dots, m\}. \quad (13)$$

In words, the lower bound for $f_m(Z_{m+1})$ in (13) is defined by shifting the deterministic upper bound downward by a constant t . The appropriate value of t guaranteeing the desired coverage for future random queries is calibrated by Algorithm 3, of which Algorithm 2 is a special case. This approach is intuitive, and it is very similar to the optimal solution of Ting (2018) for the special case of the CMS. Further, it does not require a distinct training data set, in the sense that it allows one to set $m_0^{\text{train}} = 0$ and dedicate all m_0 supervised observations with tracked frequencies to the computation of conformity scores.

The second option—which we refer to as “adaptive”—involves training, but has the advantage of being more flexible. This is inspired by the methods of Chernozhukov et al. (2021) and Sesia and Romano (2021) for regression. Concretely, consider a machine learning model that takes as input the known upper bound $\hat{f}_{\text{up}}(Z_i)$ and estimates the conditional distribution of $\hat{f}_{\text{up}}(Z_i) - f_m(Z_i)$ given $\hat{f}_{\text{up}}(Z_i)$. For example, think of a multiple quantile neural network (Taylor, 2000) or a quantile random forest (Meinshausen, 2006). After fitting this model on the m_0^{train} supervised data points (X_i, Y_i) allocated for training, let \hat{q}_t be the estimated α_t -th lower quantile of $\hat{f}_{\text{up}}(Z_i) - f_m(Z_i) \mid \hat{f}_{\text{up}}(Z_i)$, for all $t \in \{1, \dots, T\}$ and some fixed sequence $0 = \alpha_1 < \dots < \alpha_T = 1$. Without loss of generality, let $\hat{q}_0 = 0$ and $\hat{q}_T = m$. Then, define

$$\hat{L}_{m,\alpha}^{\text{adaptive}}((z, \phi); t) := \max\left\{0, \hat{f}_{\text{up}}(X_{m+1}) - \hat{q}_t\left(\hat{f}_{\text{up}}(X_{m+1})\right)\right\}, \quad t \in \{0, 1, \dots, m\}.$$

This second approach can lead to a lower bound whose distance from the upper bound is adaptive to the test instance X_{m+1} . This is an advantage, because some sketching algorithms may introduce higher uncertainty about common queries compared to rarer ones, or vice versa, and such patterns can be learnt given sufficient data. Of course, the above two examples of $\hat{L}_{m,\alpha}(\cdot; t)$ are not exhaustive. Algorithm 2 can be applied in combination with any predictor for computing nested sequences of lower bounds, and it can leverage all high-dimensional information contained in $\phi(Z_{m_0+1}, \dots, Z_m)$, not just the deterministic upper bound for the CMS and CMS-CU. However, the applications in this paper focus on the CMS and CMS-CU.

4. Confidence intervals with frequency-conditional coverage

The methodology developed in Section 3 to construct confidence intervals satisfying (8) is a non-trivial achievement on its own, but marginal coverage is not fully satisfactory for the problem considered in this paper. In fact, sketching may often involve repeated queries in practice, and certain objects may be queried more often than others. Unfortunately, marginal coverage does not guarantee that all *distinct* inferences are equally reliable. To the contrary, marginal confidence intervals for rarer queries may tend to have lower coverage, as illustrated by the following thought experiment. Imagine P_Z has support on $\mathcal{Z} = \{0, 1, 2, \dots, 10^{100}\}$, with $\mathbb{P}[Z_i = 0] = 0.95$ and $\mathbb{P}[Z_i = z] = 0.05/(|\mathcal{Z}| - 1)$ for all $z \in \mathcal{Z} \setminus \{0\}$ and $i \geq 1$. Then, one can imagine a trivial confidence interval that always contains the true frequency for a new query if $Z_{m+1} = 0$, but never has valid coverage for any other query. Such a confidence interval satisfies marginal coverage at level 95%, but it is unlikely to be very useful. This issue motivates the need for more refined conformal inference methods with stronger coverage guarantees, as discussed below.

We begin to address the limitations of marginal coverage by developing a more general method for constructing confidence intervals that are simultaneously valid for both rarer and more common random queries. Our approach is inspired by ideas from Mondrian conformal inference (Vovk et al., 2003), which have been previously used—for instance—to construct prediction sets with label-conditional coverage for classification problems (Vovk et al., 2005; Sadinle et al., 2019; Romano et al., 2020b). However, departing from the typical approach in multi-class classification, we will not seek perfect coverage conditional on the exact frequency of the queried object. In fact, that problem would be impossible to solve without stronger assumptions (Foygel Barber et al., 2021), as $f_m(Z_{m+1})$ can take a very large number of values when the sketched data set is big. Instead, we will focus on achieving a relaxed concept of frequency-conditional coverage which groups together different queries of objects that appear a similar number of times within the sketched data set.

Fix any partition $\mathcal{B} = (B_1, \dots, B_L)$ of $\{1, \dots, m\}$ into L bins such that each B_l is a sub-interval of $\{1, \dots, m\}$, for some relatively small integer L . The choice of \mathcal{B} and L will be discussed below. For the time being, it suffices to emphasize that this partition may be arbitrary, as long as it is fixed prior to seeing the data and does not depend on the new query Z_{m+1} . Our goal is to construct a confidence interval $[\hat{L}_{m,\alpha}(Z_{m+1}), \hat{U}_{m,\alpha}(Z_{m+1})]$ depending on $\phi(Z_1, \dots, Z_m)$ and \mathcal{B} that is reasonably short in practice and satisfies in theory the following notion of *frequency-range conditional coverage*:

$$\mathbb{P}[\hat{L}_{m,\alpha}(Z_{m+1}) \leq f_m(Z_{m+1}) \leq \hat{U}_{m,\alpha}(Z_{m+1}) \mid f_m(Z_{m+1}) \in B] \geq 1 - \alpha, \quad \forall B \in \mathcal{B}. \quad (14)$$

Confidence intervals satisfying (14) can be obtained by modifying Algorithm 2 as outlined in Algorithm 3. The key idea is to compute empirical quantiles for the conformity scores corresponding to the calibration data points in each frequency bin separately. Then, the final confidence interval for the random query is computed based on the largest quantile across all bins. The theoretical validity of this solution is established below in Theorem 2.

Theorem 2 *If the data Z_1, \dots, Z_{m+1} are exchangeable, the confidence interval output by Algorithm 3 satisfies the frequency-conditional property defined in (14).*

Remark. The choice of the partition \mathcal{B} involves an important trade-off. On the one side, the frequency-conditional coverage guarantee in (14) intuitively becomes stronger with

Algorithm 3 Conformalized sketching with frequency-conditional coverage

Input: Data set Z_1, \dots, Z_m . Sketching function ϕ . Warm-up period $m_0 \ll m$.
A (trainable) predictor to compute nested intervals $[\hat{L}_{m,\alpha}(\cdot; t), \hat{U}_{m,\alpha}(\cdot; t)]_{t \in \mathcal{T}}$.
Number of data points $m_0^{\text{train}} < m_0$ used for training $[\hat{L}_{m,\alpha}(\cdot; t), \hat{U}_{m,\alpha}(\cdot; t)]$.
A partition $\mathcal{B} = (B_1, \dots, B_L)$ of $\{0, \dots, m\}$ into L intervals.
Random query Z_{m+1} . Desired coverage level $1 - \alpha \in (0, 1)$.
Compute using Algorithm 1:
Data sketch ϕ ; a sparse frequency dictionary $f_{m_0}^{\text{wu}}(z), \forall z \in \mathcal{Z}$;
Variables $X_i = (Z_i, \phi(Z_{m_0+1}, \dots, Z_m))$ and $Y_i = f_{m-m_0}^{\text{sv}}(Z_i)$ for $i \in \{1, \dots, m_0\}$.
Trained predictor $[\hat{L}_{m,\alpha}(\cdot; t), \hat{U}_{m,\alpha}(\cdot; t)]$;
Conformity scores $E(X_i, Y_i)$ for all $i \in \{m_0^{\text{train}} + 1, \dots, m_0\}$.
for $i = m_0^{\text{train}} + 1, \dots, m_0$ **do**
 Assign each score $E(X_i, Y_i)$ to an appropriate frequency bin $B \in \mathcal{B}$ based on Y_i .
for $l = 1, \dots, L$ **do**
 Compute the number n_l of scores assigned to bin B_l .
 Compute $\hat{Q}_{n_l, 1-\alpha}(B_l)$ as the $\lceil (1 - \alpha)(n_l + 1) \rceil$ smallest score in bin B_l .
 Set $\hat{Q}_{n_l, 1-\alpha}^* = \max_l \hat{Q}_{n_l, 1-\alpha}(B_l)$.
 Set $X_{m+1} = (Z_{m+1}, \phi(Z_{m_0+1}, \dots, Z_m))$ as in (12).
Output: a $(1 - \alpha)$ -level confidence interval

$$\left[f_{m_0}^{\text{wu}}(Z_{m+1}) + \hat{L}_{m,\alpha}(X_{m+1}; \hat{Q}_{n_l, 1-\alpha}^*), f_{m_0}^{\text{wu}}(Z_{m+1}) + \hat{U}_{m,\alpha}(X_{m+1}; \hat{Q}_{n_l, 1-\alpha}^*) \right]$$

for the unobserved frequency $f_m(Z_{m+1})$ of Z_{m+1} defined in (2).

finer partitions; a larger value of $|\mathcal{B}|$ tends to yield more reliable confidence intervals. On the other side, coarser partitions (smaller $|\mathcal{B}|$) enable a larger number of calibration samples within each bin, leading to tighter and more stable intervals. Concretely, the applications described in this paper will adopt $|\mathcal{B}| = 5$, although finer partitions may be used when working with very large data sets. As $|\mathcal{B}|$ should remain small relative to the number m_0 of calibration samples, in general frequency-conditional coverage can only be guaranteed conditional on a relatively rough approximation of the true empirical frequency of a new query. Therefore, relatively rarer queries may still suffer from lower coverage compared to more common queries within the same frequency bin. This remaining limitation motivates the alternative approach presented below.

5. Confidence intervals with valid coverage for unique queries

5.1 Construction of confidence intervals with unique coverage

This section develops a method to construct conformal confidence intervals with guaranteed coverage for a sufficiently large fraction of unique queries in a possibly redundant test set. The following notation will be helpful to state this goal formally. Denote by \mathcal{Z}^{cal} the multiset of calibration samples Z_i for all $i \in \mathcal{I}^{\text{cal}} = \{m_0^{\text{train}} + 1, \dots, m_0\}$, for an appropriate $m_0 < m$. As above, we define n_0 as the cardinality of \mathcal{I}^{cal} . Next, define a multiset $\mathcal{Z}^{\text{test}}$ of M new queries, indexed by $\mathcal{I}^{\text{test}} = \{m + 1, \dots, m + M\}$, assumed to be sampled from P_Z

exchangeably with one another and with all other m samples. Define also $\text{UNIQUE}(\mathcal{Z}^{\text{test}}) \subseteq \mathcal{Z}^{\text{test}}$ as the unordered subset of unique objects in $\mathcal{Z}^{\text{test}}$. Then, let Z^* be a random sample from the uniform distribution over $\text{UNIQUE}(\mathcal{Z}^{\text{test}})$. In short, we may write:

$$\begin{aligned} Z_1, \dots, Z_m, Z_{m+1}, \dots, Z_{m+M} &\stackrel{\text{exch.}}{\sim} P_Z, \\ Z^* &\sim \text{Uniform}[\text{UNIQUE}(Z_{m+1}, \dots, Z_{m+M})]. \end{aligned} \quad (15)$$

The goal is to construct a confidence interval $[\hat{L}_{m,\alpha}(Z^*), \hat{U}_{m,\alpha}(Z^*)]$ satisfying:

$$\mathbb{P}^* \left[\hat{L}_{m,\alpha}(Z^*) \leq f_m(Z^*) \leq \hat{U}_{m,\alpha}(Z^*) \right] \geq 1 - \alpha, \quad (16)$$

for any desired $\alpha \in (0, 1)$. Above, the probability \mathbb{P}^* is taken with respect to Z_1, \dots, Z_{m+M} as well as to the randomness in Z^* , according to the model defined in (15). Equations (15)–(16) say that our goal is to cover at least a fraction $1 - \alpha$ of the unique queries in the test set; on average over the distribution of the test and calibration data. In the special case of a test set with cardinality $M = 1$, the property in (16) reduces to marginal coverage.

To achieve (16) with any value of M , we follow an approach inspired by Dunn et al. (2022). Randomly partition the calibration data into $G = \lfloor n_0/M \rfloor$ multisets $\mathcal{Z}_g^{\text{cal}}$, for $g \in [G]$. Without loss of generality, assume the cardinality of each $\mathcal{Z}_g^{\text{cal}}$ is M . For our method to be powerful, we will need $n_0 > M$, and ideally we would like $n_0 \gg M$; or equivalently a large G . Following the same notation as above, let $\text{UNIQUE}(\mathcal{Z}_g^{\text{cal}}) \subseteq \mathcal{Z}_g^{\text{cal}}$ denote the unordered subset of unique objects in $\mathcal{Z}_g^{\text{cal}}$, for all $g \in [G]$. Then, for each $g \in [G]$, pick an element from each $\mathcal{Z}_g^{\text{cal}}$ uniformly at random and call it $\tilde{Z}_g \in \mathcal{Z}$. By construction, the pairs $(\mathcal{Z}_g^{\text{cal}}, \tilde{Z}_g)$ are exchangeable with one another as well as with $(\mathcal{Z}^{\text{test}}, Z^*)$, for all $g \in [G]$. Therefore, a confidence interval $[\hat{L}_{m,\alpha}(Z^*), \hat{U}_{m,\alpha}(Z^*)]$ satisfying (16) can be obtained by applying the same method as in Section 3.2 with the calibration set \mathcal{Z}^{cal} replaced by $(\tilde{Z}_1, \dots, \tilde{Z}_G)$.

This solution is outlined in Algorithm 4 and its theoretical validity is established by Theorem 3. Note that Algorithm 4 is written as to potentially allow the size M' of each of the G calibration multisets to be different from the size M of the test set. This generalization of Algorithm 4 with $M' \neq M$ will be studied theoretically in the next section, and it is interesting to consider because one may sometimes be tempted to apply Algorithm 4 with $M' < M$ in practical applications with finite amounts of data. However, in the remainder of this section, we continue to focus on the standard choice of $M' = M$.

Theorem 3 *Assume that the data Z_1, \dots, Z_{m+M} are exchangeable. If Algorithm 4 is applied with parameter M' equal to the test set size M , the output confidence interval satisfies the unique-query coverage property defined in (16).*

Remark. The cardinality M of the query set controls the trade-off between the power and reliability of the confidence intervals output by Algorithm 4, assuming the latter is applied with parameter $M' = M$ as prescribed by Theorem 3. On the one hand, smaller values of M lead to tighter and more stable intervals due to a larger number G of samples available for computing the empirical quantiles of the conformity scores. On the other hand, larger values of M lead to stronger theoretical guarantees, as they further reduce the dependence between the expected conditional coverage for a particular query and the

Algorithm 4 Conformalized sketching with valid coverage for unique queries

Input: Same as for Algorithm 2, with M random queries Z_{m+1}, \dots, Z_{m+M} .
Calibration set size M' (ideally, $M' = M$).

Compute using Algorithm 1:

Data sketch ϕ ; a sparse frequency dictionary $f_{m_0}^{\text{wu}}(z), \forall z \in \mathcal{Z}$;
Variables $X_i = (Z_i, \phi(Z_{m_0+1}, \dots, Z_m))$ and $Y_i = f_{m-m_0}^{\text{sv}}(Z_i)$ for $i \in \{1, \dots, m_0\}$.
Trained predictor for computing nested intervals $[\hat{L}_{m,\alpha}(\cdot; t), \hat{U}_{m,\alpha}(\cdot; t)]$;
Conformity scores $E(X_i, Y_i)$ for all $i \in \{m_0^{\text{train}} + 1, \dots, m_0\}$.

Define $G = \lfloor n_0/M' \rfloor$, where $n_0 = m_0 - m_0^{\text{train}}$.

Partition at random $\{m_0^{\text{train}} + 1, \dots, m_0\}$ into G subsets $\mathcal{I}_g^{\text{cal}}$.

for $g = 1, \dots, G$ **do**

Pick uniformly at random one value Z_g^* from the set $\text{UNIQUE}(\{Z_i\}_{i \in \mathcal{I}_g^{\text{cal}}})$.

Set $X_g^* = (Z_g^*, \phi(Z_{m_0+1}, \dots, Z_m))$ as in (12), and $Y_g^* = f_{m-m_0}^{\text{sv}}(Z_g^*)$.

Set $E_g^* = E(X_g^*, Y_g^*)$.

Compute $\hat{Q}_{G,1-\alpha}$ as the $\lceil (1-\alpha)(G+1) \rceil$ smallest score in $\{E_g^*\}_{g=1}^G$.

Pick Z^* uniformly at random from $\text{UNIQUE}(\{Z_{m+1}, \dots, Z_{m+M}\})$.

Set $X^* = (Z^*, \phi(Z_{m_0+1}, \dots, Z_m))$ as in (12).

Output: a $(1-\alpha)$ -level confidence interval

$$\left[f_{m_0}^{\text{wu}}(Z^*) + \hat{L}_{m,\alpha}(X^*; \hat{Q}_{n_0,1-\alpha}^*), f_{m_0}^{\text{wu}}(Z^*) + \hat{U}_{m,\alpha}(X^*; \hat{Q}_{n_0,1-\alpha}^*) \right]$$

for the unobserved frequency $f_m(Z^*)$ of Z^* defined in (2).

population frequency of that query. In general, we recommend that Algorithm 4 should be applied with values of M so large as to result in a number G of final calibration samples in the hundreds. Concretely, the numerical experiments presented in this paper will apply Algorithm 4 with values of M allowing $G > 100$.

We conclude this section by emphasizing that Algorithm 4 and Algorithm 3 differ in their formally stated goals (achieving unique-query coverage and frequency-conditional coverage, respectively), but they are designed to mitigate the same limitation of confidence intervals with marginal coverage. On the one hand, unique-query coverage is intuitively more appealing and easier to explain compared to frequency-conditional coverage, as anticipated in Section 4. On the other hand, Algorithm 4 is also quite data-expensive (as is Algorithm 3), in the sense that it requires a calibration set that is large relative to the size of the query set. Therefore, the relative advantages of Algorithms 3 and 4 in finite samples may not necessarily be straightforward to see, suggesting the need for a deeper theoretical study of Algorithm 4 (in the remainder of this section) as well as careful simulations (in Section 6).

5.2 Robustness to sample inflation

To better understand Algorithm 4, we study the robustness of its unique coverage guarantee in settings where our method is not applied exactly as prescribed by the theory. In particular, we are interested in understanding what happens if the test sample size M is larger than the size M' of the available calibration subsets $\mathcal{Z}_g^{\text{cal}}$, for all $g \in [G]$.

Let us begin the analysis by recalling the key modelling assumption used throughout this paper: all data points are sampled exchangeably from a discrete distribution P_Z with support on some countable dictionary \mathcal{Z} . To facilitate the analysis hereafter, we further assume that the data are not only exchangeable but also independent; that is, $Z_i \stackrel{\text{i.i.d.}}{\sim} P_Z$, for all $i \in [m + M]$. Denote $P_Z = \sum_{j \in \mathbb{N}} p_j \delta_{a_j}$, where the $a_j \in \mathcal{Z}$ are the distinct symbols in the dictionary \mathcal{Z} , while $p_j > 0$ for all $j \in \mathbb{N}$ and $\sum_{j \in \mathbb{N}} p_j = 1$. Note that a discrete data distribution is a natural assumption in the context of sketching—practical hashing computations can only operate with discrete values—and it is the only interesting case to consider in a theoretical analysis of Algorithm 4. In fact, the set of unique values in any finite sample from a continuous distribution is almost surely the same as the original sample.

Let $V = \text{UNIQUE}(\mathcal{Z}^{\text{test}})$ denote the set of unique values in the test set $\mathcal{Z}^{\text{test}}$, which contains all Z_i indexed by $i \in \mathcal{I}^{\text{test}}$. For any positive integers k and M such that $M \geq k$, let $C_{M,k}$ be the set of k -compositions of M : these are the sequences $c = (c_1, \dots, c_k)$ of positive integers $c_j \geq 1$ such that $\sum_{j=1}^k c_j = M$. It is known that the number of such sequences is $|C_{M,k}| = \binom{M-1}{k-1}$; e.g., Riordan (2012). With this notation, we can characterize the probability distribution of the set V of unique values among a random sample from P_Z ; see Proposition A9 in Appendix B. From there, we obtain the following result characterizing the distribution $U_Z^{[M]}$ of a uniformly sampled element ζ over the set of uniques V , when $V \sim P_Z^{[M]}$. This result will be useful in our analysis of the robustness of Algorithm 4 to situations in which $M' \neq M$.

Proposition 4 (Uniform distribution over unique elements) *Let $\mathcal{Z}^{\text{test}}$ be an i.i.d. sample of size M from a discrete distribution $P_Z = \sum_{i \in \mathbb{N}} p_j \delta_{a_j}$, where $a_j \in \mathcal{Z}$ are distinct, and $p_j > 0$ for all $j \in \mathbb{N}$. Let $U_Z^{[M]}$ be the distribution of a uniformly sampled element ζ of $V = \text{UNIQUE}(\mathcal{Z}^{\text{test}})$. Then, for all $j_1 \in \mathbb{N}$, the probability mass function of ζ at a_{j_1} is*

$$U_Z^{[M]}(\zeta = a_{j_1}) = \sum_{k=1}^M \frac{1}{k} \sum_{J=\{j_1, \dots, j_k\} \subset \mathbb{N}^k, |J|=k} \sum_{c \in C_{M,k}} \binom{M}{c_1 \ c_2 \ \dots \ c_k} p_{j_1}^{c_1} \cdots p_{j_k}^{c_k}. \quad (17)$$

In particular, $U_Z^{[1]} = U_Z^{[2]} = P_Z$, and for all $j_1 \in \mathbb{N}$,

$$U_Z^{[3]}(\zeta = a_{j_1}) = \frac{p_{j_1}(2p_{j_1}^2 - 3p_{j_1} + 3)}{2} + \frac{p_{j_1}}{2} \sum_{\{j_2, j_3\} \subset (\mathbb{N} \setminus \{j_1\})^2, |J|=2} p_{j_2} p_{j_3}.$$

Proposition 4 suggests that one should generally expect to lose coverage over unique queries when applying Algorithm 4 with a calibration set size M' that is different from the size M of the test set. Indeed, the $U_Z^{[M]}$ -probability of the event $\zeta = a_j$ can either increase or decrease as a function of M , depending on the probability p_j of a_j under P_Z . To see this, define the function $\tau : [0, 1] \rightarrow [0, 1]$, such that for all $p \in [0, 1]$,

$$\tau(p) = \frac{p(2p^2 - 3p + 3)}{2}. \quad (18)$$

A plot of τ is in Figure A7 (a), Appendix E. Then, for P_Z taking only two possible distinct values a_1 and a_2 , with probabilities p_1 and p_2 , respectively, Proposition 4 implies that for

$j = 1, 2$, $U_Z^{[3]}(\zeta = a_j) = \tau(p_j)$. Now, for $p \in [0, 1/2)$, $\tau(p) < p$, while for $p \in (1/2, 1]$, $\tau(p) > p$. Assuming $p_1 < p_2$, we have $U_Z^{[3]}(\zeta = a_1) < U_Z^{[2]}(\zeta = a_1)$, while $U_Z^{[3]}(\zeta = a_2) > U_Z^{[2]}(\zeta = a_2)$. Thus, the probability of $\zeta = a_i$ can either increase or decrease as a function of M , depending on p_j . Hence, we expect that the probability of the coverage event using calibration samples of size M' , which is a union of such elementary events, can also increase or decrease as a function of M .

More specifically, let $\mathcal{E} = \{\hat{L}_{m,\alpha}(Z^*) \leq f_m(Z^*) \leq \hat{U}_{m,\alpha}(Z^*)\}$ be the coverage event from (16), whose probability is lower bounded in Theorem 3. Let the random variables Z_i , $i \in \mathcal{I}^{\text{cal}}$ (calibration sets of size M') and $i \in \mathcal{I}^{\text{test}}$ (a test set of size M) be i.i.d. according to P_Z . The probability of coverage can be written in terms of the variables \tilde{Z}_g , for $g \in [G]$, which are i.i.d. following the distribution $U_Z^{[M']}$ —abbreviated as $\tilde{Z}_{1:G} \sim (U_Z^{[M']})^{|G|}$ —and an independent random variable Z^* , which follows the distribution $U_Z^{[M]}$, as

$$\mathbb{P}_{Z^* \sim U_Z^{[M]}, \tilde{Z}_{1:G} \sim (U_Z^{[M']})^{|G|}}[\mathcal{E}] = \mathbb{E}_{Z^* \sim U_Z^{[M]}} \mathbb{P}_{\tilde{Z}_{1:G} \sim (U_Z^{[M']})^{|G|}}[\mathcal{E}] = \mathbb{E}_{Z^* \sim U_Z^{[M]}} e(Z^*). \quad (19)$$

Above, we defined $e(Z^*) = \mathbb{P}_{\tilde{Z}_{1:G} \sim (U_Z^{[M']})^{|G|}}[\mathcal{E}]$ to be the conditional probability of the coverage event \mathcal{E} , given Z^* . Theorem 3 tells us that the expectation in (19) is at least $1 - \alpha$ if $M' = M$. However, when $M' \neq M$, we have showed that $U_Z^{[M']}$ can be different from $U_Z^{[M]}$. Thus the above expectation of $e(Z^*)$ may decrease, and the method may lose coverage.

Aiming to understand the extent by which the coverage can be affected, we let $\mathcal{P}_{\mathbb{N}}(\mathcal{Z}; K)$ be the set of discrete probability distributions over \mathcal{Z} supported on at most K distinct values. Then, we introduce the quantity

$$\Delta(M, M'; K) = \sup_{P_Z \in \mathcal{P}_{\mathbb{N}}(\mathcal{Z}; K)} \sup_{j \in \mathbb{N}} \left| U_Z^{[M]}(\{a_j\}) - U_Z^{[M']}(\{a_j\}) \right|,$$

which measures the worst-case difference between the probabilities of observing a value a_j according to the distributions $U_Z^{[M]}$ and $U_Z^{[M']}$. Here, we are thinking of $U_Z^{[M]}$ as the calibration distribution and $U_Z^{[M']}$ as the test distribution. Thus, if our conformal prediction algorithm outputs sets of size at most $s \geq 0$, then the probability of those sets differs by at most $s \cdot \Delta(M, M'; K)$ between the training at test distributions.

Studying $\Delta(M, M'; K)$ seems quite challenging in general, as it involves maximizing differences of probabilities given in (17). These are nontrivial quantities to deal with, because (a) large values of M lead to large-degree polynomials in the expressions for the p_j -s, and (b) large values of K lead to large numbers of degrees of freedom (i.e., many different p_j -s). Therefore, we restrict our analysis to the simpler but still non-trivial special case of $K = 2$; i.e., we imagine there are only two distinct objects in the population P_Z .

To do this, we can assume without loss of generality that $M > M'$, as Δ is symmetric in M, M' . Moreover, we can also assume without loss of generality that $M' \geq 2$, since $U_Z^{[1]} = U_Z^{[2]}$ and thus the cases $M' = 1$ and $M' = 2$ are equivalent. For fixed $M > M' \geq 2$, we will need the function $h : [0, \infty) \rightarrow \mathbb{R}$ defined, for all $\delta \in [0, \infty)$, as

$$h(\delta) = \ln \frac{1 + \delta^{M-1}}{1 + \delta^{M'-1}} - (M - M') \ln(1 + \delta). \quad (20)$$

Our next result characterizes $\Delta(M, M'; 2)$ based on the function h . The proof relies on carefully studying the monotonicity properties of Δ using calculus; see Section C.7.

Proposition 5 (Characterizing $\Delta(M, M'; 2)$) Fix $M > M' \geq 2$ and take the function h as defined in (20). There is a unique solution $\delta_* \in [0, 1]$ to $h(\delta_*) = \ln(M'/M)$, and

$$\Delta(M, M'; 2) = \frac{1}{2} \left| \frac{1 - \delta_*^M}{(1 + \delta_*)^M} - \frac{1 - \delta_*^{M'}}{(1 + \delta_*)^{M'}} \right|.$$

As an illustration, we consider the setting where $M = aM'$, for some $a > 1$. This corresponds to applying Algorithm 4 using calibration multisets of size M' , with M' being smaller than the target test set size M by a factor $1/a$. Naturally, one would like to know how low the coverage may be in this case compared to the ideal situation in which $M' = M$. Our next result shows the loss in coverage may remain relatively contained, as long as a is moderate and M is large. The proof leverages Proposition 5 and relies on a detailed analysis of the polynomial equation satisfied by the maximizing δ , see Section C.8.

Corollary 6 (Asymptotics of $\Delta(M, M/a; 2)$) As $M \rightarrow \infty$, with $\nu(a) := a^{-\frac{1}{a-1}}(1 - \frac{1}{a})$,

$$\left| \frac{\Delta(M, M/a; 2)}{\nu(a)} - 1 \right| = O(1/M).$$

Combined with (19) and Theorem 3, Corollary 6 implies that the coverage over unique values for a test set of size M and calibration sets of size $M' = M/a$ satisfies, for large M ,

$$\mathbb{P}_{Z^* \sim U_Z^{[M]}, \tilde{Z}_{1:G} \sim (U_Z^{[Ma]})_{|G|}}[\mathcal{E}] \geq 1 - \alpha - 2 \cdot \nu(a) - O\left(\frac{1}{M}\right).$$

This immediately gives the following result, which sheds some light on the behaviour of Algorithm 4 when applied with $M' \neq M$.

Theorem 7 Assume that the data Z_1, \dots, Z_{m+M} are exchangeable and imagine Algorithm 4 is applied at the nominal coverage level $\alpha \in (0, 1)$ with parameter $M' = M/a$ for some $a > 1$, where M is the size of the test set. Then, the output confidence interval satisfies the unique-query coverage property defined in (16) at level $\alpha + 2 \cdot \nu(a) + O(1/M)$, where $\nu(a) := a^{-1/(a-1)}(1 - 1/a)$.

To better understand this result, it helps to look at the plot of the function ν shown in Figure A7 (b). For instance, if $a = 1.2$, we have $\nu(a) \approx 0.067$; therefore, a 95% nominal coverage level may result empirical coverage over unique queries that is as low as 80.6% when $M = 100$. If $a = 1.1$, we have $\nu(a) \approx 0.035$; therefore, a 95% nominal coverage level may result empirical coverage over unique queries that is as low as 87.0% when $M = 100$. Of course, Theorem 7 only gives us a lower bound for the coverage over unique queries which refers to the worst-case scenario over all data distributions P_Z . In practice, Algorithm 4 applied with $M' < M$ may sometimes result in higher coverage than anticipated by Theorem 7, as we will demonstrate empirically in Section 6.

5.3 Robustness to distribution shift

An additional advantage of the unique-query coverage property defined in (15) is that it tends to be more “robust” to certain types of distribution shift compared to the standard notion of marginal coverage. In other words, if Algorithm 4 is applied in a situation where the queried objects are not sampled from the same distribution as the sketched data, its effective coverage over unique queries may be lower than the ideal $1 - \alpha$ expected under perfect exchangeability, but this loss may not be as large as that of Algorithm 2. Specifically, the next result establishes that, in the special case of $K = 2$ studied above, the probabilities shift less in the worst case under the distribution $U_Z^{[M]}$ of unique values than under the original distribution P_Z , for a large range of probability values p_i of P_Z . The proof relies on the mean value theorem and can be found in Section C.10.

Theorem 8 (Bounding the effect of distribution shift) *Let Z and Z' take two values with probabilities p_1, p_2 , and p'_1, p'_2 , respectively. For $M \geq 3$, let $U_Z^{[M]}$ be the distribution of a uniformly sampled element over $\text{UNIQUE}(V)$, when $V \sim P_Z^{[M]}$; and define $U_{Z'}^{[M]}$ similarly. Define $c \in (0, 1/2)$ as the unique solution of*

$$c^{M-1} + (1 - c)^{M-1} = \frac{2}{M}. \quad (21)$$

Let

$$S_c = \{P = (p_1, p_2) : p_j \in (c, 1 - c), j = 1, 2\}.$$

Then, for all $P_Z, P_{Z'} \in S_c$, with $P_Z \neq P_{Z'}$,

$$\sup_{\mathcal{E} \subset \{a_1, a_2\}^{|G|+1}} \left| \mathbb{P}_{Z^* \sim U_Z^{[M]}, \tilde{Z}_{1:G} \sim (U_Z^{[M]})^{|G|}[\mathcal{E}]} - \mathbb{P}_{Z^* \sim U_{Z'}^{[M]}, \tilde{Z}_{1:G} \sim (U_{Z'}^{[M]})^{|G|}[\mathcal{E}]} \right| < \sup_{\mathcal{E} \subset \{a_1, a_2\}^{|G|+1}} \left| \mathbb{P}_{Z^* \sim P_Z, \tilde{Z}_{1:G} \sim P_Z^{|G|}[\mathcal{E}]} - \mathbb{P}_{Z^* \sim P_{Z'}, \tilde{Z}_{1:G} \sim P_{Z'}^{|G|}[\mathcal{E}]} \right|.$$

In other words, Theorem 8 tells us that the coverage of the sets output by Algorithm 4 tends to be relatively stable for certain classes of data distributions P_Z . Specifically, for a given P_Z , the change in coverage when shifting from the distribution of uniques $U_Z^{[M]}$ to the distribution of uniques $U_{Z'}^{[M]}$ is strictly smaller, in the worst case, than the corresponding change in coverage when shifting from P_Z to $P_{Z'}$. This suggests that Algorithm 4 may be relatively robust to distribution shifts in the query set.

Now, we can try to better understand the family of P_Z over which the distribution of unique values is more stable. Since $c < 1/2$, we have $c < 1 - c$; thus, it follows from (21) that $(1 - c)^{M-1} \leq 2/M \leq 2(1 - c)^{M-1}$, which can be rearranged to obtain:

$$1 - (2/M)^{1/(M-1)} \leq c \leq 1 - (1/M)^{1/(M-1)}.$$

Therefore, $c = O(M^{-1} \ln M)$ for large M . This implies that the distribution $U_Z^{[M]}$ of the unique values is less affected by changes in the distribution of probabilities in P_Z than P_Z itself, for a large range of possible values of p_j from $O(M^{-1} \ln M)$ to $1 - O(M^{-1} \ln M)$.

While Theorem 8 focuses on a special case in which the data distribution P_Z has support on only two possible objects in order to simplify the theoretical analysis, the relative robustness of Algorithm 4 to distribution shift in more general settings is supported by empirical experiments, as shown in Section 6.

6. Experiments and applications

6.1 Experiments with synthetic data sets

The performance of Algorithm 3 is investigated on synthetic data using the two types of conformity scores described in Section 3.3, focusing on one-sided confidence intervals. Additional experiments involving two-sided intervals are described in Appendix D. The adaptive scores used in this section are based on an isotonic distributional regression model (Henzi et al., 2021). The goal is to compute lower frequency bounds for random queries based on data compressed by the CMS-CU, implemented with $d = 3$ hash functions of width $w = 1000$. In particular, $m = 100,000$ observations are sampled i.i.d. from some distribution specified below. The first $m_0 = 5000$ observations are stored without loss during the warm-up phase, while the remaining 95,000 are compressed by the CMS-CU.

The conformity scores are evaluated separately within $L = 5$ frequency bins, seeking frequency-range conditional coverage (14). The bins are determined so that each contains approximately the same probability mass, by partitioning the range of frequencies for the objects tracked exactly according to the observed empirical quantiles. Lower bounds for new queries are computed for 10,000 i.i.d. samples from the same distribution. The quality of these bounds is quantified with two metrics: the mean *length* of the resulting confidence intervals and the *empirical coverage*—the proportion of queries for which the true frequency is covered. These performance metrics are averaged over 10 independent experiments.

Experiments are performed on synthetic data sampled from two families of distributions. First, we consider a Zipf distribution with $\mathbb{P}[Z_i = z] = z^{-a}/\zeta(a)$ for all $z \in \{1, 2, \dots\}$, where ζ is the Riemann Zeta function and $a > 1$ is a control parameter affecting the power-law tail behavior. Second, we generate synthetic data from a random probability measure distributed as the Pitman-Yor prior (Pitman and Yor, 1997) with a standard Gaussian base distribution and parameters $\lambda > 0$ and $\sigma \in [0, 1)$, as explained in Appendix A.4. The parameter λ is set to $\lambda = 5000$, while σ is varied. For $\sigma = 0$ the Pitman-Yor prior reduces to the Dirichlet prior (Ferguson, 1973), while $\sigma > 0$ results in heavier tails.

Three benchmark methods are considered. The first one is the *classical* 95% lower bound from (4). The second one is the *Bayesian* method of Cai et al. (2018), which assumes a non-parametric Dirichlet process prior for the distribution of the data stream, estimates its scaling parameter by maximizing the marginal likelihood of the observed sketch, and then computes the posterior of the queried frequencies conditional on the observed sketch. The performance of the lower 5% posterior quantile is compared to the lower bounds obtained with the other methods according to the frequentist metrics defined above. The third benchmark is the bootstrap method of Ting (2018), which is nearly exact and optimal for the vanilla CMS (up to some finite-sample discrepancy between the bootstrap and population distributions) but is not theoretically valid for other sketching techniques.

Figure 1 compares the performance of the conformal method to those of the three benchmarks on the Zipf data. All methods achieve marginal coverage (5), with the exception of the Bayesian approach whose prior is misspecified in this case. The length of the confidence intervals indicates the classical bound is very conservative, while the bootstrap and conformal methods provide relatively informative bounds, particularly when a is larger and hash collisions become rarer. The standard errors are too small to be clearly visible in this figure, and hence they are omitted.

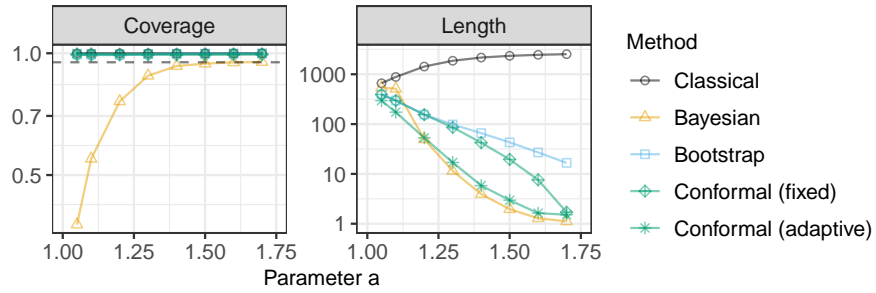


Figure 1: Performance of 95% confidence intervals with simulated Zipf data sketched with CMS-CU. The results are shown as a function of the Zipf tail parameter a .

These results also show our conformal intervals can be the shortest among all alternatives, especially if implemented with the adaptive conformity scores. This should not be surprising because the bootstrap may not be optimal for the non-linear CMS-CU algorithm. Figure 2 compares the performance of all confidence intervals in these experiments stratified by the true empirical frequency of each random query. These results show that our method applied with adaptive conformity scores leads to much tighter confidence intervals for common queries, as the underlying machine learning model is able to powerfully leverage the non-linear nature of the CMS-CU. Further, Figure 2 confirms that Algorithm 3 can construct reliable confidence intervals for both rarer and more common queries, as it controls frequency-conditional coverage (14)

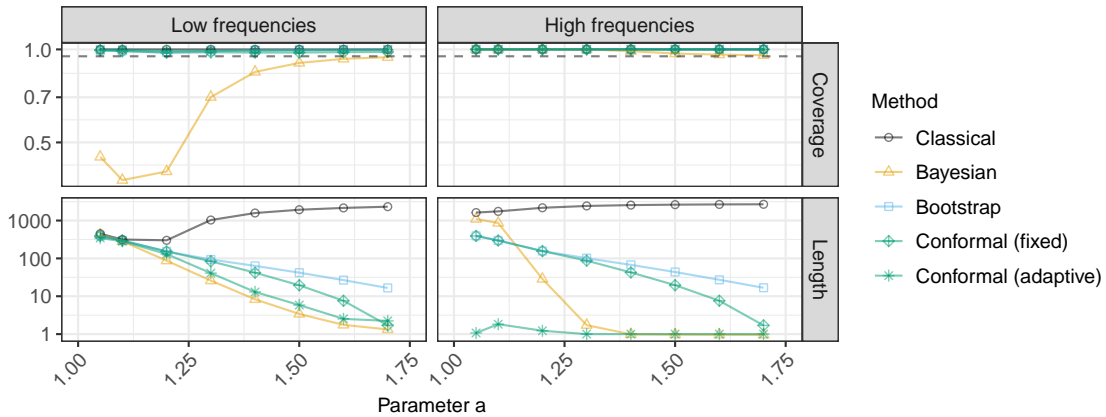


Figure 2: Performance of confidence intervals stratified by the true query frequency. Left: frequency below median; right: above median. Other details are as in Figure 1.

Supplementary results reported in Appendix E show the CMS-CU leads to more precise queries with all methods compared to the vanilla CMS; see Figure A8. Figure A9 confirms that conformal lower bounds no longer have a clear advantage over the bootstrap ones if the data are sketched with the vanilla CMS instead of the CMS-CU. In fact, although the conformal intervals obtained with the adaptive conformity scores can be a little shorter than the bootstrap ones even for the vanilla CMS, the latter have the advantage of (approximately, in the limit of large samples) satisfying an even stronger frequency-conditional coverage property equivalent to (14) with bins of size 1 (Ting, 2018). Analogous results for the experiments with Pitman-Yor process data are also in Appendix E; see Figures A10–A13.

Figure 3 reports on additional experiments demonstrating the performance of Algorithm 4 for constructing confidence intervals with valid coverage for unique queries at level $1 - \alpha = 95\%$. These experiments follow the same setup as those in Figure 1, simulating data from a Zipf distribution with tail parameter 1.5. The difference is that the coverage and length performance metrics are now averaged only on the unique objects $\text{UNIQUE}(\mathcal{Z}^{\text{test}})$ in a set $\mathcal{Z}^{\text{test}}$ containing $M = 100$ independent random queries. Algorithm 4 is applied using fixed conformity scores and different values of M' , which controls the size of the calibration subsets, ranging from 1 to 100.

Unsurprisingly, the desired 95% coverage for unique queries (16) is achieved when $M' \approx M$, as anticipated by Theorem 3. By contrast, the coverage for unique queries is lower than 95% when M' is small. This should not be surprising because Algorithm 4 reduces to Algorithm 2 if $M' = 1$, and the latter is designed to provide marginal coverage (5), not coverage for unique queries (16). In fact, as shown in Figure A14, even Algorithm 3, which is designed to achieve the relatively stronger notion of frequency-range conditional coverage (14), does not always provide valid inference for unique queries. Finally, Figure 3 also highlights that the unique-query coverage practically achieved by applying on these data Algorithm 4 with smaller values of M' is much higher than the worst-case asymptotic lower bound, $\max(0, 1 - \alpha - 2 \cdot \nu(100/M'))$, given by Theorem 7.

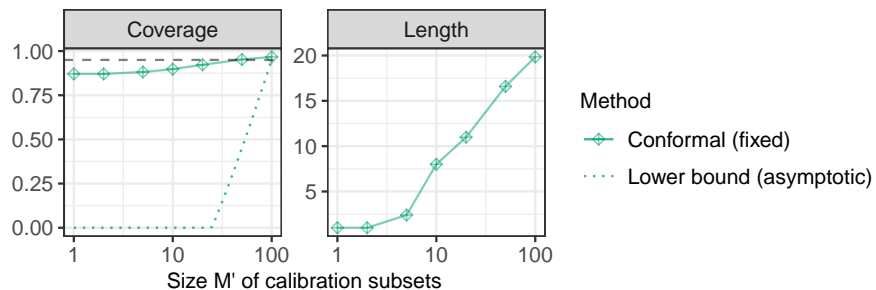


Figure 3: Performance of confidence intervals for unique queries in a test set of size 100, as a function of the parameter M' of Algorithm 4 for constructing conformal confidence intervals satisfying (16). Other details are as in Figure 1.

Figure 4 reports on experiments investigating empirically the robustness of the conformal confidence intervals output by Algorithms 2 and 4 to distribution shifts in the query set.

These experiments follow the same setup as those in Figure 3, simulating data from a Zipf distribution with different values of the tail parameter. However, the difference is that now the $M = 100$ random test queries are sampled from a mixture distribution with two components. The first component is the same Zipf distribution from which the sketched data are generated, while the second component is an independent continuous uniform distribution on $[0, 1]$. This setup is designed to study the effects of an extreme form of distributional shift, as objects sampled from the second component of the mixture are almost surely unique (up to rounding errors at machine precision) and are never previously observed in the integer-valued sketched data set. The mixing proportion serves as a control parameter and it is varied from zero (no distribution shift) to unity (full shift). Note that this setup is not inconsistent with the original assumption from Section 1.2 that the data distribution has support on a discrete set \mathcal{X} , because in truth even (approximately) uniform random numbers on a computer are discrete (they are finitely long binary sequences).

The performance of the conformal confidence intervals output by Algorithm 2, applied with fixed conformity scores, is measured in terms of average coverage and length over all random queries in the test set. By contrast, the performance of the conformal confidence intervals output by Algorithm 4, also applied with fixed conformity scores, is measured in terms of average coverage and length over the unique queries in the test set. Such choice is useful to facilitate the validation of Theorem 8, which suggests Algorithm 2 should be relatively robust to distribution shifts by these metrics. Indeed, the empirical results confirm the unique coverage guarantee provided by Algorithm 4 is more robust to distribution shifts compared to the marginal coverage property sought by Algorithm 2, although the performances of both methods in this setting also depend on the distribution of the sketched data. In particular, it is interesting to note that lower values of the Zipf tail parameter lead to larger numbers of unique objects in the queried data, increasing the robustness of all conformal confidence intervals to distribution shifts corresponding to unusually high proportions of new queries in the test set.

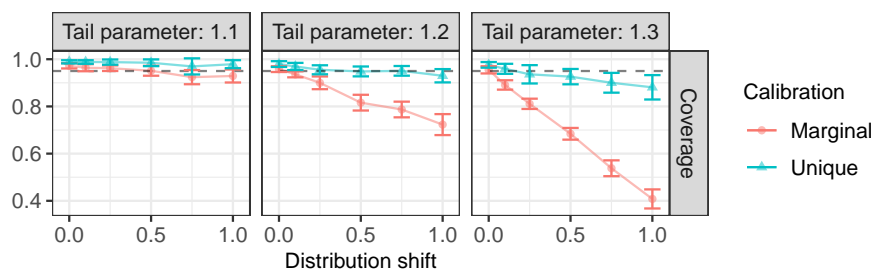


Figure 4: Performance of conformal confidence intervals with marginal (Algorithm 2) or unique-query (Algorithm 4) coverage in a test set of size $M = 100$ with varying degrees of distribution shift. Other details are as in Figure 1.

6.2 Analysis of 16-mers in SARS-CoV-2 DNA sequences

This application involves a data set of nucleotide sequences from SARS-CoV-2 viruses made publicly available by the National Center for Biotechnology Information (Hatcher et al., 2017). The data include 43,196 sequences, each consisting of approximately 30,000 nucleotides. The goal is to estimate the empirical frequency of each *16-mer*, a distinct sequence of 16 DNA bases in contiguous nucleotides. Given that each nucleotide has one of 4 bases, there are $4^{16} \approx 4.3$ billion possible 16-mers. Thus, exact tracking of all 16-mers is not unfeasible, which allows us to validate the sketch-based queries. Sequences containing missing values are removed during pre-processing, for simplicity.

The experiments are carried out as in Section 6.1, processing the 16-mers in a random order to ensure their exchangeability. However, a larger sample of size 1,000,000 is sketched, and the width w of the hash functions is varied. Figure 5 compares the performances of all methods as a function of the hash width, in terms of marginal coverage and mean confidence interval width. All methods achieve the desired marginal coverage, except for the Bayesian approach when w is large. For small w , all methods return intervals of similar width, because the distribution of SARS-CoV-2 16-mers frequencies is quite concentrated with relatively narrow support (Figure A15), which makes it especially difficult to compress the data without much loss. By contrast, the proposed conformal methods yield noticeably shorter confidence intervals if w is large. Figure A16 reports the same results stratified by the frequency of the queried objects, while Figure A17 confirms the advantage of sketching with the CMS-CU as opposed to the vanilla CMS. Table A1 lists 10 common and 10 rare queries along with their corresponding deterministic upper bounds for $w = 50,000$, comparing the lower bounds obtained with each method. Table A2 shows analogous results with $w = 5,000$.

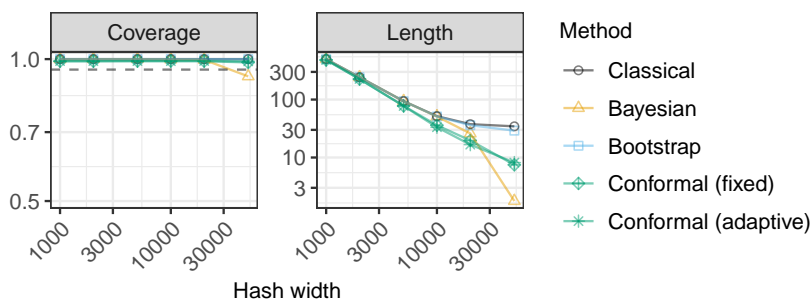


Figure 5: Performance of confidence intervals based on SARS-CoV-2 sequence data. The results are shown as a function of the hash width. Other details are as in Figure 1.

Figure A18 compares the performances of different frequency *point-estimates* in terms of mean absolute deviation from the true frequency. With the classical method, we take the midpoint of the 95% confidence interval as a point estimate, although other approaches are also possible (Cormode and Yi, 2020). For the other methods, the point estimate is the lower confidence bound at level $\alpha = 0.5$; in the Bayesian case, this is the posterior median. Although a conformal lower bound with $\alpha = 0.5$ is not always a reliable estimator

of conditional medians (Medarametla and Candès, 2021), this approach outperformed the benchmarks in all of our experiments.

Figure A19 shows the confidence intervals reported in Figure 5 approximately remain valid even if their average coverage is evaluated with respect to unique queries only; of course, this is not guaranteed in general. Figure A20 shows the performance of the procedure described in Algorithm 4 for constructing conformal confidence intervals with valid coverage for unique queries. These results show that Algorithm 4 leads to valid inference across a wide range of values of its parameter M' —the size of the calibration subsets—despite the more pessimistic worst-case predictions of Theorem 7. Finally, Figure A21 investigates the robustness of the alternative types of conformal prediction intervals output by Algorithm 2 and Algorithm 4 to distribution shifts in the test queries, similarly to Figure 4.

6.3 Analysis of 2-grams in English literature

This application is based on data consisting of 18 open-domain pieces of classic English literature downloaded from the Gutenberg Corpus (Project Gutenberg, 1971-present) using the NLTK Python package (Bird et al., 2009). The goal is to count the frequencies of all *2-grams*—consecutive pairs of English words. After basic pre-processing to remove punctuation and unusual words (only those in a relatively small dictionary of 25,487 common English words are retained), the number of 2-grams remaining in this data set is approximately 1,700,000 (the total number of all *possible* 2-grams within this dictionary is approximately 650,000,000). Note that such pre-processing does not remove very common words (such as “the”, “or”, etc.) and it may sometimes lead to unnatural 2-grams whenever a relatively rare word is removed from an otherwise meaningful sentence (e.g., “very uncommon for” would become “very for”). Therefore, our analysis is not fully realistic from a natural language processing perspective but it is computationally efficient and still informative regarding the performance of our uncertainty estimation method. With this setup, the same experiments are then carried out as in Section 6.2, sketching 1,000,000 randomly sampled 2-grams and querying 10,000 independent 2-grams. As in the previous experiments, the 2-grams are processed in a random order to ensure exchangeability.

Figure 6 shows the conformal intervals produced by Algorithm 3 using adaptive scores achieve the desired 95% marginal coverage and tend to have the shortest width. By contrast, the Bayesian intervals are not valid unless the hashes are very wide. Here, the conformal approach enjoys a larger improvement in performance compared to the other approaches because these data can be compressed efficiently due to the weaker power-law tail behavior of the frequency distribution of English 2-grams; see Figure A15. Figures A22–A24 and Tables A1–A2 report additional results along the lines of those in the previous section, including empirical evidence of valid frequency-conditional coverage.

Figure A25 shows the confidence intervals reported in Figure 6 approximately remain valid even if their average coverage is evaluated with respect to unique queries only; of course, this is not guaranteed in general. Figure A26 illustrates the performance of Algorithm 4, showing that valid inference for unique queries can be achieved with a wide range of the parameter M' , despite the more pessimistic worst-case predictions of Theorem 7. Finally, Figure A27 investigates the robustness of the alternative types of conformal intervals output by Algorithms 2 and 4 to distribution shifts in the test queries, similarly to Figure 4.

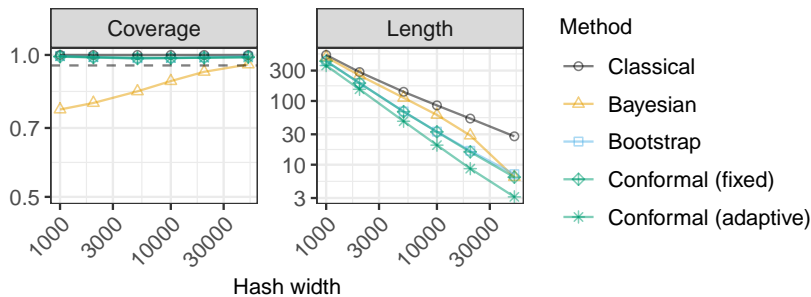


Figure 6: Performance of confidence intervals for random queries, for a sketched data set of English 2-grams in classic English literature. Other details are as in Figure 5.

7. Discussion

Conformalized sketching is a non-parametric and data-adaptive method for quantifying uncertainty in problems involving frequency estimation from sketched data. This paper has revolved around the CMS, and variations thereof, because that is a prominent sketching algorithm for which several statistical benchmarks are available. However, our conformal inference approach is very broadly applicable because it does not require any knowledge of the sketching algorithm nor any parametric assumptions about the data distribution.

Conformal inference generally rests on data exchangeability; this assumption may not always be appropriate in the context of sketching, but it is a reasonable approximation in many relevant applications. For example, in natural language processing one may wish to count the frequencies of non-contiguous tuples of words co-occurring in the same sentence within a large corpus, expanding on the example of Section 6.3. In that case, sketching is useful because it could be computationally unfeasible to track all frequencies exactly, and the exchangeability assumption is reasonable as long as the tuples are processed and queried in a random order. That being said, this paper has taken several steps in Sections 4 and 5 to mitigate the susceptibility of the “vanilla” conformalized sketching method described in Section 3 to possible violations of the data exchangeability assumption.

Finally, this work opens new opportunities for further research. For example, in the future one may study and compare theoretically, in some settings, the length of our conformal confidence intervals under different types of coverage guarantees. A possible approach to this problem may take inspiration from relevant work in the context of regression by Lei et al. (2018) and Sesia and Candès (2020). Further, it would be interesting to explore the relevance of the novel methods and theory presented in Section 5 beyond the sketching problem considered in this paper. For example, the results of Section 5 could be easily repurposed to construct conformal prediction sets for regression or multi-class classification tasks that achieve valid coverage over subsets of individual test cases with certain unique attributes. In those contexts, our work may lead to a useful alternative framework for dealing with problems of uncertainty estimation under algorithmic fairness constraints (Romano et al., 2020a) or stratified sampling mechanisms (Dunn et al., 2022; Park et al., 2022).

Software and computations

Accompanying software and data are available online at <https://github.com/msesia/conformalized-sketching>. Experiments were carried out in parallel on a computing cluster; each experiment required less than a few hours with a standard CPU and less than 5GB of memory (20 GB are needed for the analysis of the SARS-CoV-2 DNA data).

Acknowledgements

M. S. is supported in part by NSF grant DMS 2210637 and by an Amazon Research Award. S. F. is also affiliated to IMATI-CNR “Enrico Magenes” (Milan, Italy), and received funding from the European Research Council under the European Union’s Horizon 2020 research and innovation program under grant 817257. E. D. is supported in part by the NSF DMS 2046874 (CAREER) award, and ONR grant N00014-21-1-2843.

References

- A. N. Angelopoulos, S. Bates, M. I. Jordan, and J. Malik. Uncertainty sets for image classifiers using conformal prediction. In *9th International Conference on Learning Representations, 2021, Virtual Event, Austria, May 3-7, 2021*, 2021.
- S. Bates, E. Candès, L. Lei, Y. Romano, and M. Sesia. Testing for outliers with conformal p-values. *preprint at arXiv:2104.08279*, 2021.
- S. Bird, E. Klein, and E. Loper. *Natural language processing with Python: analyzing text with the natural language toolkit*. ” O’Reilly Media, Inc.”, 2009.
- D. Cai, M. Mitzenmacher, and R. P. Adams. A Bayesian nonparametric view on count-min sketch. In *Advances in Neural Information Processing Systems 31*, pages 8782–8791, 2018.
- E. Candès, L. Lei, and Z. Ren. Conformalized survival analysis. *arXiv preprint arXiv:2103.09763*, 2021.
- M. Charikar, K. Chen, and M. Farach-Colton. Finding frequent items in data streams. In *International Colloquium on Automata, Languages, and Programming*, pages 693–703. Springer, 2002.
- V. Chernozhukov, K. Wüthrich, and Y. Zhu. Distributional conformal prediction. *Proceedings of the National Academy of Sciences*, 118(48), 2021.
- G. Cormode and S. Muthukrishnan. An improved data stream summary: the count-min sketch and its applications. *Journal of Algorithms*, 55(1):58–75, 2005.
- G. Cormode and K. Yi. *Small summaries for big data*. Cambridge University Press, 2020.
- G. Cormode, S. Jha, T. Kulkarni, N. Li, D. Srivastava, and T. Wang. Privacy at scale: Local differential privacy in practice. In *Proceedings of the 2018 International Conference on Management of Data*, pages 1655–1658, 2018.

- E. Dobriban and S. Liu. Asymptotics for sketching in least squares regression. In *Advances in Neural Information Processing Systems*, pages 3675–3685, 2019.
- E. Dolera, S. Favaro, and S. Peluchetti. A Bayesian nonparametric approach to count-min sketch under power-law data streams. In *International Conference on Artificial Intelligence and Statistics*, pages 226–234. PMLR, 2021.
- P. Drineas and M. W. Mahoney. RandNLA: randomized numerical linear algebra. *Communications of the ACM*, 59(6):80–90, 2016.
- R. Dunn, L. Wasserman, and A. Ramdas. Distribution-free prediction sets for two-layer hierarchical models. *Journal of the American Statistical Association*, 0(0):1–12, 2022.
- C. Estan and G. Varghese. New directions in traffic measurement and accounting. In *Proceedings of the 2002 conference on Applications, technologies, architectures, and protocols for computer communications*, pages 323–336, 2002.
- L. Fan, P. Cao, J. Almeida, and A. Z. Broder. Summary cache: a scalable wide-area web cache sharing protocol. *IEEE/ACM transactions on networking*, 8(3):281–293, 2000.
- S. T. Ferguson. A Bayesian analysis of some nonparametric problems. *The Annals of Statistics*, 1:209–230, 1973.
- R. Foygel Barber, E. J. Candes, A. Ramdas, and R. J. Tibshirani. The limits of distribution-free conditional predictive inference. *Information and Inference: A Journal of the IMA*, 10(2):455–482, 2021.
- S. Geisser. *Predictive inference: an introduction*. Chapman and Hall/CRC, 2017.
- A. Goyal and H. Daumé. Lossy conservative update (lcu) sketch: Succinct approximate count storage. In *Proceedings of the AAAI Conference on Artificial Intelligence*, volume 25, pages 878–883, 2011.
- A. Goyal, H. Daumé III, and G. Cormode. Sketch algorithms for estimating point queries in nlp. In *Proceedings of the 2012 joint conference on empirical methods in natural language processing and computational natural language learning*, pages 1093–1103, 2012.
- C. Gupta, A. K. Kuchibhotla, and A. K. Ramdas. Nested conformal prediction and quantile out-of-bag ensemble methods. *Pattern Recognition*, 127, 2022.
- N. Halko, P.-G. Martinsson, and J. A. Tropp. Finding structure with randomness: Probabilistic algorithms for constructing approximate matrix decompositions. *SIAM review*, 53(2):217–288, 2011.
- E. L. Hatcher, S. A. Zhdanov, Y. Bao, O. Blinkova, E. P. Nawrocki, Y. Ostapchuck, A. A. Schäffer, and J. R. Brister. Virus variation resource—improved response to emergent viral outbreaks. *Nucleic acids research*, 45(D1):D482–D490, 2017.
- A. Henzi, J. F. Ziegel, and T. Gneiting. Isotonic distributional regression. *Journal of the Royal Statistical Society: Series B (Statistical Methodology)*, 83(5):963–993, 2021.

- C.-Y. Hsu, P. Indyk, D. Katabi, and A. Vakilian. Learning-based frequency estimation algorithms. In *International Conference on Learning Representations*, 2019.
- R. Izbicki, G. T. Shimizu, and R. B. Stern. Flexible distribution-free conditional predictive bands using density estimators. *preprint at arXiv:1910.05575*, 2019.
- T. Jiang, Y. Li, H. Lin, Y. Ruan, and D. P. Woodruff. Learning-augmented data stream algorithms. In *International Conference on Learning Representations*, 2019.
- R. Kaur, S. Jha, A. Roy, S. Park, E. Dobriban, O. Sokolsky, and I. Lee. iDECODe: In-distribution equivariance for conformal out-of-distribution detection. *Association for the Advancement of Artificial Intelligence (AAAI)*, 2022.
- C. Kockan, K. Zhu, N. Dokmai, N. Karpov, M. O. Kulekci, D. P. Woodruff, and S. C. Sahinalp. Sketching algorithms for genomic data analysis and querying in a secure enclave. *Nature methods*, 17(3):295–301, 2020.
- K. Krishnamoorthy and T. Mathew. *Statistical tolerance regions: theory, applications, and computation*. John Wiley & Sons, 2009.
- J. Lacotte and M. Pilanci. Optimal randomized first-order methods for least-squares problems. In *International Conference on Machine Learning*, pages 5587–5597. PMLR, 2020.
- J. Lei and L. Wasserman. Distribution-free prediction bands for non-parametric regression. *Journal of the Royal Statistical Society: Series B (Statistical Methodology)*, 76(1):71–96, 2014.
- J. Lei, J. Robins, and L. Wasserman. Distribution-free prediction sets. *Journal of the American Statistical Association*, 108(501):278–287, 2013.
- J. Lei, M. G’Sell, A. Rinaldo, R. J. Tibshirani, and L. Wasserman. Distribution-free predictive inference for regression. *Journal of the American Statistical Association*, 113(523):1094–1111, 2018.
- L. Lei, E. J. Candès, et al. Conformal inference of counterfactuals and individual treatment effects. *Journal of the Royal Statistical Society Series B*, 83(5):911–938, 2021.
- S. Li, X. Ji, E. Dobriban, O. Sokolsky, and I. Lee. PAC-Wrap: Semi-supervised PAC anomaly detection. *KDD 2022, arXiv preprint arXiv:2205.10798*, 2022.
- S. Liu and E. Dobriban. Ridge regression: Structure, cross-validation, and sketching. *arXiv preprint arXiv:1910.02373, International Conference on Learning Representations (ICLR) 2020*, 2019.
- M. W. Mahoney. Randomized algorithms for matrices and data. *Foundations and Trends in Machine Learning*, 3(2):123–224, 2011.
- P.-G. Martinsson and J. A. Tropp. Randomized numerical linear algebra: Foundations and algorithms. *Acta Numerica*, 29:403–572, 2020.

- D. Medarametla and E. Candès. Distribution-free conditional median inference. *Electronic Journal of Statistics*, 15(2):4625–4658, 2021.
- N. Meinshausen. Quantile regression forests. *Journal of Machine Learning Research*, 7: 983–999, 2006.
- J. Misra and D. Gries. Finding repeated elements. *Science of computer programming*, 2(2): 143–152, 1982.
- H. Papadopoulos, K. Proedrou, V. Vovk, and A. Gammerman. Inductive confidence machines for regression. In *European Conference on Machine Learning*, pages 345–356. Springer, 2002.
- S. Park, E. Dobriban, I. Lee, and O. Bastani. Pac prediction sets under covariate shift. *International Conference on Learning Representations (ICLR) 2022*, 2021.
- S. Park, E. Dobriban, I. Lee, and O. Bastani. Pac prediction sets for meta-learning. In *Advances in Neural Information Processing Systems*, 2022.
- G. Pitel and G. Fouquier. Count-min-log sketch: Approximately counting with approximate counters. *arXiv preprint arXiv:1502.04885*, 2015.
- J. Pitman and M. Yor. The two parameter poisson-dirichlet distribution derived from a stable subordinator. *The Annals of Probability*, 25:855–900, 1997.
- Project Gutenberg. Project Gutenberg. www.gutenberg.org, 1971-present. Accessed: 2022-02-05.
- H. Qiu, E. Dobriban, and E. Tchetgen Tchetgen. Distribution-free prediction sets adaptive to unknown covariate shift. *arXiv preprint arXiv:2203.06126*, 2022.
- J. Riordan. *Introduction to combinatorial analysis*. Courier Corporation, 2012.
- Y. Romano, E. Patterson, and E. Candès. Conformalized quantile regression. In *Advances in Neural Information Processing Systems*, pages 3538–3548, 2019.
- Y. Romano, R. F. Barber, C. Sabatti, and E. Candès. With Malice Toward None: Assessing Uncertainty via Equalized Coverage. *Harvard Data Science Review*, 2(2), apr 30 2020a. <https://hdr.mitpress.mit.edu/pub/qedrwcz3>.
- Y. Romano, M. Sesia, and E. Candès. Classification with valid and adaptive coverage. *Advances in Neural Information Processing Systems*, 33:3581–3591, 2020b.
- M. Sadinle, J. Lei, and L. Wasserman. Least ambiguous set-valued classifiers with bounded error levels. *Journal of the American Statistical Association*, 114(525):223–234, 2019.
- C. Saunders, A. Gammerman, and V. Vovk. Transduction with confidence and credibility. In *IJCAI*, 1999.
- S. Schechter, C. Herley, and M. Mitzenmacher. Popularity is everything: A new approach to protecting passwords from {Statistical-Guessing} attacks. In *5th USENIX Workshop on Hot Topics in Security (HotSec 10)*, 2010.

- H. Scheffe and J. W. Tukey. Non-parametric estimation. i. validation of order statistics. *The Annals of Mathematical Statistics*, 16(2):187–192, 1945.
- M. Sesia and E. J. Candès. A comparison of some conformal quantile regression methods. *Stat*, 9(1):e261, 2020.
- M. Sesia and S. Favaro. Conformal frequency estimation with sketched data. *arXiv preprint arXiv:2204.04270*, 2022.
- M. Sesia and Y. Romano. Conformal prediction using conditional histograms. *Advances in Neural Information Processing Systems*, 34, 2021.
- Q. Shi, J. Petterson, G. Dror, J. Langford, A. Smola, and S. Vishwanathan. Hash kernels for structured data. *Journal of Machine Learning Research*, 10(11), 2009.
- J. W. Taylor. A quantile regression neural network approach to estimating the conditional density of multiperiod returns. *Journal of Forecasting*, 19(4):299–311, 2000.
- D. Ting. Count-min: Optimal estimation and tight error bounds using empirical error distributions. In *Proceedings of the 24th ACM SIGKDD International Conference on Knowledge Discovery & Data Mining*, pages 2319–2328, 2018.
- J. W. Tukey. Non-parametric estimation ii. statistically equivalent blocks and tolerance regions—the continuous case. *The Annals of Mathematical Statistics*, pages 529–539, 1947.
- J. W. Tukey. Nonparametric estimation, iii. statistically equivalent blocks and multivariate tolerance regions—the discontinuous case. *The Annals of Mathematical Statistics*, pages 30–39, 1948.
- S. S. Vempala. *The random projection method*, volume 65. American Mathematical Soc., 2005.
- V. Vovk. Cross-conformal predictors. *Annals of Mathematics and Artificial Intelligence*, 74(1-2):9–28, 2015.
- V. Vovk, D. Lindsay, I. Nourtdinov, and A. Gammerman. Mondrian confidence machine. Technical report, Royal Holloway, University of London, 2003.
- V. Vovk, A. Gammerman, and G. Shafer. *Algorithmic learning in a random world*. Springer, 2005.
- V. Vovk, I. Nourtdinov, and A. Gammerman. On-line predictive linear regression. *Annals of Statistics*, 37(3):1566–1590, 2009.
- A. Wald. An Extension of Wilks’ Method for Setting Tolerance Limits. *The Annals of Mathematical Statistics*, 14(1):45–55, 1943.
- S. S. Wilks. Determination of Sample Sizes for Setting Tolerance Limits. *The Annals of Mathematical Statistics*, 12(1):91–96, 1941.

- D. P. Woodruff. Sketching as a tool for numerical linear algebra. *Foundations and Trends in Theoretical Computer Science*, 10(1–2):1–157, 2014.
- F. Yang, S. Liu, E. Dobriban, and D. P. Woodruff. How to reduce dimension with pca and random projections? *IEEE Transactions on Information Theory*, 67(12):8154–8189, 2021.
- Q. Zhang, J. Pell, R. Canino-Koning, A. C. Howe, and C. T. Brown. These are not the k-mers you are looking for: efficient online k-mer counting using a probabilistic data structure. *PloS one*, 9(7):e101271, 2014.

A. Additional methodological details

A.1 The CMS algorithm

Algorithm A5 CMS

Input: Data Z_1, \dots, Z_m . Sketch dimensions d, w . Hash functions h_1, \dots, h_d . Query z .
Initialize: $C_{j,k} = 0$ for all $j \in [d], k \in [w]$.
for $i = 1, \dots, m$ **do**
 for $j = 1, \dots, d$ **do**
 Increment $C_{j,h_j(Z_i)} \leftarrow C_{j,h_j(Z_i)} + 1$
 Compute $\hat{f}_{\text{up}}^{\text{CMS}}(z) = \min_{j \in [d]} \{C_{j,h_j(z)}\}$.
Output: deterministic upper-bound for the frequency of z in the data set: $\hat{f}_{\text{up}}^{\text{CMS}}(z)$.

A.2 The CMS-CU algorithm

Algorithm A6 CMS-CU

Input: Data Z_1, \dots, Z_m . Sketch dimensions d, w . Hash functions h_1, \dots, h_d . Query z .
Initialize: $C_{j,k} = 0$ for all $j \in [d], k \in [w]$.
for $i = 1, \dots, m$ **do**
 Compute $j^* = \arg \min_{j \in [d]} C_{j,h_j(Z_i)}$.
 Increment $C_{j^*,h_{j^*}(Z_i)} \leftarrow C_{j^*,h_{j^*}(Z_i)} + 1$
 Compute $\hat{f}_{\text{up}}^{\text{CMS-CU}}(z) = \min_{j \in [d]} \{C_{j,h_j(z)}\}$.
Output: deterministic upper-bound for the frequency of z in the data set: $\hat{f}_{\text{up}}^{\text{CMS-CU}}(z)$.

A.3 Constructing two-sided conformal confidence intervals

This section describes two alternative methods for constructing two-sided conformal confidence intervals. The first method, explained in Section A.3.1, consists of directly calibrating a sequence of nested two-sided intervals, as outlined in Section 3.2. The second method, explained in Section A.3.2, consists of separately calibrating two sequences of lower and upper one-sided confidence intervals, each adopting the significance level $\alpha/2$ instead of α . The second approach is easier to implement compared to the first one, building upon the techniques detailed earlier in this paper, but it may be less statistically efficient.

A.3.1 CONSTRUCTION BASED ON CONDITIONAL HISTOGRAMS

Two-sided conformal confidence intervals for $f_m(X_{m+1})$ can be constructed by following the general recipe outlined in Section 3.2. To implement this method practically, one needs to fix an increasing sequence of candidate intervals $[\hat{L}_{m,\alpha}(\cdot; t), \hat{U}_{m,\alpha}(\cdot; t)]$, depending on Z_{m+1} and $\phi(Z_{m_0+1}, \dots, Z_m)$. Possible choices for such sequence may be directly borrowed from the existing literature on conformal inference for regression, including for example the quantile regression approach of Romano et al. (2019) or the conditional histogram approach of Sesia and Romano (2021). Here, we describe a particular implementation that combines the idea in Sesia and Romano (2021) with a Bayesian model, in continuity with the works of Cai et al. (2018) and Dolera et al. (2021) on Bayesian empirical frequency estimation from sketched data. However, the same idea could easily accommodate a quantile regression model or any other machine learning algorithm instead of the Bayesian model, as explained in Sesia and Romano (2021). Note that the following paragraphs largely retrace the same steps as in Sesia and Romano (2021), which are however useful to recap here to make the presentation self contained.

For any $j \in [m]$, let $\hat{\varphi}_j(x)$ indicate the posterior probability of $f_m(X_{m+1}) = j$ for $X_{m+1} = x$ as estimated by any Bayesian model for frequency estimation given sketched data, such as that of Cai et al. (2018) based on a Dirichlet process prior, for example. For convenience of notation, we will sometimes refer to the full posterior distribution of $f_m(X_{m+1})$ simply as $\hat{\varphi}$. Note that, in general, the form of the posterior distribution $\hat{\varphi}$ may depend on m as well as on the sketched data in $\phi(Z_{m_0+1}, \dots, Z_m)$. Following in the footsteps of Sesia and Romano (2021), define the following bi-valued function \mathcal{S} taking as input a query x , the posterior distribution $\hat{\varphi}$, a scalar threshold $t \in [0, 1]$, and two intervals $S^-, S^+ \subseteq \{1, \dots, m\}$:

$$\mathcal{S}(x, \hat{\varphi}, S^-, S^+, t) := \arg \min_{(l,u) \in \{1, \dots, m\}^2 : l \leq u} \left\{ |u - l| : \sum_{j=l}^u \hat{\varphi}_j(x) \geq t, S^- \subseteq [l, u] \subseteq S^+ \right\}. \quad (22)$$

Above, it is implied that we choose the value of (l, u) minimizing $\sum_{j=l}^u \hat{\varphi}_j(x)$ among the feasible ones with minimal $|u - l|$, whenever the optimization problem does not have a unique solution. Therefore, we can assume without loss of generality that (22) has a unique solution; if that is not the case, we can break the ties at random by adding a little noise to $\hat{\varphi}$. As explained in Sesia and Romano (2021), the problem defined in (22) can be solved efficiently, at computational cost linear in m . Note that we will sometimes refer to sub-intervals of $[m]$ as either contiguous subsets of $\{1, \dots, m\}$ (e.g., S^-) or as pairs of lower and upper endpoints (e.g., $[l, u]$).

If $S^- = \emptyset$ and $S^+ = \{1, \dots, m\}$, the expression in (22) computes the shortest interval with total posterior probability mass above t . In general, the optimization in (22) involves the additional *nesting* constraint that the output \mathcal{S} must satisfy $S^- \subseteq \mathcal{S} \subseteq S^+$, which will be needed to guarantee the resulting sequence of confidence intervals indexed by t is nested. Note that the inequality in (22) involving t may not be binding at the optimal solution due to the discrete nature of the optimization problem. However, the above construction could be easily modified by introducing some suitable randomization leading to confidence intervals that are even tighter on average, as explained in Sesia and Romano (2021).

For any integer $T \geq 1$, consider an increasing sequence $t_\tau \in [0, 1]$, for $\tau \in \{0, \dots, T\}$. A nested sequence of T intervals indexed by $\tau \in \{0, \dots, T\}$, which may be written as

$$S_t = [\hat{L}_{m,\alpha}(X_{m+1}; t_\tau), \hat{U}_{m,\alpha}(X_{m+1}; t_\tau)],$$

for appropriate endpoints $\hat{L}_{m,\alpha}(X_{m+1}; t_\tau)$ and $\hat{U}_{m,\alpha}(X_{m+1}; t_\tau)$, respectively, is then constructed from (22) as follows. First, fix any *starting index* $\bar{\tau} \in \{0, 1, \dots, T\}$ and define $S_{\bar{\tau}}$ by applying (22) without the nesting constraints (with $S^- = \emptyset$ and $S^+ = \{1, \dots, m\}$):

$$S_{\bar{\tau}} := \mathcal{S}(x, \hat{\varphi}, \emptyset, \{1, \dots, m\}, t_{\bar{\tau}}), \quad (23)$$

Note the explicit dependence on x and $\hat{\varphi}$ of the left-hand-side above is omitted for simplicity, although it is important to keep in mind that $S_{\bar{\tau}}$ does of course depend on these quantities.

Having computed the initial interval $S_{\bar{\tau}}$, we recursively extend the definition to the wider intervals indexed by $\tau = \bar{\tau} + 1, \dots, T$ as follows:

$$S_\tau := \mathcal{S}(x, \hat{\varphi}, S_{\tau-1}, \{1, \dots, m\}, t_\tau).$$

See Sesia and Romano (2021) for a schematic visualization of this step. Similarly, the narrower intervals S_τ indexed by $\tau = \bar{\tau} - 1, \bar{\tau} - 2, \dots, 0$ are defined recursively as:

$$S_\tau := \mathcal{S}(x, \hat{\varphi}, \emptyset, S_{\tau+1}, t_\tau).$$

See Sesia and Romano (2021) for a schematic visualization of this step. As a result of this construction, the sequence of intervals $\{S_\tau\}_{\tau=0}^T$ is nested regardless of the starting point $\bar{\tau}$ in (23), for which a typical choice is such that $t_{\bar{\tau}} = 1 - \alpha$. Then, two-sided conformal confidence intervals for $f_m(X_{m+1})$ can be obtained by applying Algorithm 2 with this particular sequence of input nested intervals. We refer to Sesia and Romano (2021) for further details on the construction of nested intervals outlined above.

A.3.2 CONSTRUCTION BASED ON BONFERRONI CORRECTION

An alternative, and somewhat simpler, approach to building two-sided conformal confidence intervals for $f_m(X_{m+1})$ at level $1 - \alpha$ consists of constructing a pair of lower and upper one-sided confidence intervals at level $1 - \alpha/2$. In particular, consider the following two nested sequences S_t^l and S_t^u of one-sided confidence intervals, each indexed by a scalar parameter t :

$$S_t^l = [\hat{L}_{m,\alpha/2}(X_{m+1}; t), \hat{f}_{\text{up}}^{\text{CMS}}(X_{m+1})], \quad S_t^u = [0, \hat{U}_{m,\alpha/2}(X_{m+1}; t)],$$

where $\hat{f}_{\text{up}}^{\text{CMS}}(X_{m+1})$ is a deterministic upper bound for the unknown true empirical frequency of X_{m+1} ; e.g., see Section 1.2. The sequences S_t^l and S_t^u can be separately calibrated using the conformal inference method described in Sections 3.2 and 3.3, for any given choice of frequency-range partition \mathcal{B} , as we shall make more precise below. This gives two distinct data-adaptive thresholds $\hat{Q}_{n,1-\alpha/2}^{*,l}$ and $\hat{Q}_{n,1-\alpha/2}^{*,u}$, respectively, such that, $\forall B \in \mathcal{B}$,

$$\mathbb{P} \left[f_m(X_{m+1}) \geq \hat{L}_{m,\alpha/2}(X_{m+1}; \hat{Q}_{n,1-\alpha/2}^{*,l}) \mid f_m(Z_{m+1}) \in B \right] \geq 1 - \frac{\alpha}{2},$$

and

$$\mathbb{P} \left[f_m(X_{m+1}) \leq \hat{U}_{m,\alpha/2}(X_{m+1}; \hat{Q}_{n,1-\alpha/2}^{*,u}) \mid f_m(Z_{m+1}) \in B \right] \geq 1 - \frac{\alpha}{2}.$$

By a union bound, we obtain that the following two-sided conformal confidence interval has valid coverage, in the sense of (14), at level $1 - \alpha$:

$$[\hat{L}_{m,\alpha/2}(X_{m+1}; \hat{Q}_{n,1-\alpha/2}^{*,l}), \hat{U}_{m,\alpha/2}(X_{m+1}; \hat{Q}_{n,1-\alpha/2}^{*,u})].$$

Different practical implementations are available to construct the sequences of candidate lower bounds $\hat{L}_{m,\alpha/2}(X_{m+1}; t)$ and upper bounds $\hat{U}_{m,\alpha/2}(X_{m+1}; t)$. Two concrete examples are explained below.

Constant conformity scores. A simple option to construct $\hat{L}_{m,\alpha/2}(X_{m+1}; t)$ is to directly apply the method described in Section 3.3, for example by shifting $\hat{f}_{\text{up}}^{\text{CMS}}(X_{m+1})$ downward by a constant t . Then, the conformalized threshold $\hat{Q}_{n,1-\alpha/2}^{*,l}$ can be calibrated exactly as described in Section 3.2. The sequence of candidate upper bounds $\hat{U}_{m,\alpha/2}(X_{m+1}; t)$ can also be constructed similarly to $\hat{L}_{m,\alpha/2}(X_{m+1}; t)$, for example by adding a constant t to the trivial lower bound of 0, up to the deterministic upper bound $\hat{f}_{\text{up}}^{\text{CMS}}(X_{m+1})$. The threshold $\hat{Q}_{n,1-\alpha/2}^{*,u}$ for $\hat{U}_{m,\alpha/2}(X_{m+1}; t)$ can then be calibrated as usual with Algorithm 2.

Bootstrap conformity scores. An alternative option to construct the sequence $\hat{L}_{m,\alpha/2}(X_{m+1}; t)$ consists of shifting downward by a constant t the bootstrap lower bound calculated with the method of Ting (2018), at level $\alpha/2$. Similarly, the sequence $\hat{U}_{m,\alpha/2}(X_{m+1}; t)$ can be obtained by shifting upward by a constant t the analogous bootstrap upper bound at level $1 - \alpha/2$. Thus, in the special case of the vanilla CMS, our conformal confidence intervals based on these scores intuitively become very similar to the bootstrap confidence intervals of Ting (2018). In general, however, the difference remains that the intervals of Ting (2018) rely on the linearity of the CMS, while ours are theoretically valid regardless of how the data are sketched. We have observed this option works well in practice, at least within the scope of our numerical experiments. Therefore, this is the implementation adopted in our numerical experiments described in Section D.

A.4 Sampling from a Pitman-Yor predictive distribution

The data points are sampled sequentially from the following predictive distribution, which has parameters $\lambda > 0$ and $\sigma \in [0, 1)$. After sampling Z_1 from a standard normal distribution, $\mathcal{N}(0, 1)$, fix any $i \geq 1$ and let Z_1, \dots, Z_i indicate the data stream observed up to that point. Denote by k_i the number of distinct elements within it, and by $V_i = (V_{i,1}, \dots, V_{i,k_i})$ the set of such distinct values. Further, let $c_{i,l}$ indicate the number of times that object $V_{i,l}$ has been observed in Z_1, \dots, Z_i , for $l \in \{1, \dots, k_i\}$. Then, Z_{i+1} is generated as follows:

$$Z_{i+1} \mid Z_1, \dots, Z_i = \begin{cases} V_{i,l}, & \text{with probability } \frac{c_{i,l} - \sigma}{\lambda + i}, \text{ for } l \in \{1, \dots, k_i\}, \\ \mathcal{N}(0, 1), & \text{with probability } \frac{\lambda + k_i \sigma}{\lambda + i}. \end{cases}$$

Above, the second case which occurs with probability $(\lambda + k_i \sigma) / (\lambda + i)$ corresponds to sampling a new unique value from the standard normal distribution.

B. Auxiliary theoretical results

B.1 Probability distribution of the set of uniques

Note that the size of V is between 1 and M ; and the values taken by V range over subsets $\{a_{j_1}, \dots, a_{j_k}\} \subseteq \mathcal{Z}$, where $1 \leq k \leq M$ and $j_1, \dots, j_k \in \mathbb{N}$ are distinct indices.

Proposition A9 (Probability distribution of the set of uniques) *Let \mathcal{Z}^{test} be an i.i.d. sample of size M from a discrete distribution $P_Z = \sum_{i \in \mathbb{N}} p_j \delta_{a_j}$, where $a_j \in \mathcal{Z}$ are distinct, and $p_j > 0$ for all $j \in \mathbb{N}$. Let $P_Z^{[M]}$ be the probability distribution of \mathcal{Z}^{test} . Let $V = \text{UNIQUE}(\mathcal{Z}^{test})$ denote the set of unique values in \mathcal{Z}^{test} . For any $1 \leq k \leq M$, and any distinct indices $j_1, \dots, j_k \in \mathbb{N}$, the probability mass function of V at $\{a_{j_1}, \dots, a_{j_k}\}$ equals*

$$P_Z^{[M]}(V = \{a_{j_1}, \dots, a_{j_k}\}) = \sum_{c \in C_{M,k}} \binom{M}{c_1 \ c_2 \ \dots \ c_k} p_{j_1}^{c_1} \cdots p_{j_k}^{c_k} \quad (24)$$

$$= \sum_{S \subset \{j_1, \dots, j_k\}} (-1)^{k+|S|} \left(\sum_{j \in S} p_j \right)^M. \quad (25)$$

The proof of (24) follows directly from the definitions, while that of (25) relies on a careful combinatorial argument, pairing sets of odd and even sizes; see Appendix C.5.

To better understand (24), consider the trivial example in which $M = 1$; in this case, $P_Z^{[1]}(V = \{a_j\}) = p_j$ for all $j \in \mathbb{N}$. Thus, $P_Z^{[1]}$, the distribution of uniques when sampling a single element from the distribution P_Z , is equal precisely to P_Z itself; i.e., $P_Z^{[1]} = P_Z$. For $M = 2$, we have that $P_Z^{[2]}(V = \{a_j\}) = p_j^2$ for all $j \in \mathbb{N}$; this is the probability of observing a_i twice in a row. Further, for all $j_1, j_2 \in \mathbb{N}$ with $j_1 \neq j_2$, we have that $P_Z^{[2]}(V = \{a_{j_1}, a_{j_2}\}) = 2p_{j_1}p_{j_2}$; this is the probability of observing (a_{j_1}, a_{j_2}) or (a_{j_2}, a_{j_1}) , so that the set of uniques is $\{a_{j_1}, a_{j_2}\}$. One can also verify that (25) leads to the same results. Continuing the above example, for $M = 2$, for all $j_1, j_2 \in \mathbb{N}$ with $j_1 \neq j_2$, (25) leads to $P_Z^{[2]}(V = \{a_{j_1}, a_{j_2}\}) = (p_{j_1} + p_{j_2})^2 - p_{j_1}^2 - p_{j_2}^2 = 2p_{j_1}p_{j_2}$, agreeing with (24).

C. Mathematical proofs

C.1 Proof of Proposition 1

Proof Consider $((X_{\pi(1)}, Y_{\pi(1)}), \dots, (X_{\pi(m_0)}, Y_{\pi(m_0)}), (X_{\pi(m+1)}, Y_{\pi(m+1)}))$ for any permutation π of $\{1, \dots, m_0, m+1\}$. This is equal to $((X'_1, Y'_1), \dots, (X'_{m_0}, Y'_{m_0}), (X'_{m+1}, Y'_{m+1}))$, defined by applying the functions in (11)–(12) to a shuffled data set $Z_{\tilde{\pi}(1)}, \dots, Z_{\tilde{\pi}(m+1)}$, where $\tilde{\pi}$ indicates a permutation of $\{1, \dots, m+1\}$ that agrees with π on $\{1, \dots, m_0, m+1\}$ and leaves $\{m_0+1, \dots, m\}$ unchanged. Therefore,

$$\begin{aligned} & ((X_{\pi(1)}, Y_{\pi(1)}), \dots, (X_{\pi(m_0)}, Y_{\pi(m_0)}), (X_{\pi(m+1)}, Y_{\pi(m+1)})) \\ &= ((X'_1, Y'_1), \dots, (X'_{m_0}, Y'_{m_0}), (X'_{m+1}, Y'_{m+1})) \\ &\stackrel{d}{=} ((X_1, Y_1), \dots, (X_{m_0}, Y_{m_0}), (X_{m+1}, Y_{m+1})), \end{aligned}$$

where the last equality in distribution follows directly from the assumption that Z_1, \dots, Z_{m+1} are exchangeable. \blacksquare

C.2 Proof of Theorem 1

Proof We refer to the proof of the more general Theorem 2, of which this result is a special case. In fact, Algorithm 2 corresponds to Algorithm 3 applied with trivial partitions that divide the range of frequencies into a single bin: $L = 1$. Further, the marginal coverage property in (8) is a special case of the frequency-conditional coverage property in (14) with the trivial partitions corresponding to $L = 1$. \blacksquare

C.3 Proof of Theorem 2

The following notation will be helpful: let $B(Y_i) \in \mathcal{B}$ indicate the frequency bin into which Y_i belongs, for $i \in \{1, \dots, m_0, m+1\}$. We begin by proving the result for the simpler case in which Algorithm 2 is applied using conformity scores that do not require training, in which case $m_0^{\text{train}} = 0$. For $i \in \{1, \dots, m_0, m+1\}$, define the random variables Y_i and X_i as in (11)–(12), respectively. We already know from Proposition 1 that $(X_1, Y_1), \dots, (X_{m_0}, Y_{m_0}), (X_{m+1}, Y_{m+1})$ are exchangeable. This implies that the conformity scores $E(X_i, Y_i)$ are exchangeable with one another, for $i \in \{1, \dots, m_0, m+1\}$, because each of them only depends on X_i, Y_i and on the separate data points in the sketch $\phi(Z_{m_0+1}, \dots, Z_m)$. Therefore, E_{m+1} is also exchangeable with the subset of conformity scores with indices in $\{i \in \{1, \dots, m_0\} : B(Y_i) = B(Y_{m+1})\}$.

Now, fix any bin $B^* \in \mathcal{B}$ and assume $B(Y_{m+1}) = B^*$. Now, note that the interval output by Algorithm 2 does not cover the true frequency $f_m(Z_{m+1})$ if and only if $E_{m+1} > \hat{Q}_{n, 1-\alpha} \geq \hat{Q}_{n_i, 1-\alpha}(B^*)$. However, a standard exchangeability argument for the conformity scores in $\{i \in \{1, \dots, m_0\} : B(Y_i) = B^*\}$ shows that $\mathbb{P}[E_{m+1} > \hat{Q}_{n_i, 1-\alpha}(B^*) \mid B(Y_{m+1}) = B^*] \leq 1 - \alpha$; for example, see Lemma 1 of Romano et al. (2019). This completes the first part of the proof.

The second part with $m_0^{\text{train}} > 0$ follows very similarly: Proposition 1 implies that $(X_{m_0^{\text{train}}+1}, Y_{m_0^{\text{train}}+1}), \dots, (X_{m_0}, Y_{m_0}), (X_{m+1}, Y_{m+1})$ are exchangeable, and so must be the conformity scores E_i for $i \in \{m_0^{\text{train}}+1, \dots, m_0, m+1\}$ because each of them only depends on the corresponding X_i, Y_i and on the separate set of observations indexed by $\{1, \dots, m_0^{\text{train}}\}$, as well as on the sketch $\phi(Z_{m_0+1}, \dots, Z_m)$. The rest of the proof is exactly the same as in the first part because the empirical quantiles $\hat{Q}_{n_i, 1-\alpha}(B)$ are only computed on subsets of the data indexed by $\{m_0^{\text{train}}+1, \dots, m_0\}$.

C.4 Proof of Theorem 3

Following the same notation as in Algorithm 4, let Z^* indicate a random object sampled uniformly from $\text{UNIQUE}(\{Z_{m+1}, \dots, Z_{m+M}\})$. Define also $X^* = (Z^*, \phi(Z_{m_0+1}, \dots, Z_m))$. By construction, Z^* is exchangeable with all Z_g^* for $g \in [G]$, and X^* is exchangeable with all X_g^* for $g \in [G]$. This implies that the conformity scores $E_g^* = E(X_g^*, Y_g^*)$ are exchangeable

with one another, for all $g \in [G]$, as well as with $E^* = E(X^*, Y^*)$. The result is then established with the same argument as in the proof of Theorem 2. The true frequency $f_m(Z^*)$ is not covered by the output confidence interval if and only if $E^* > \hat{Q}_{G,1-\alpha}$, whose probability is bound from above by $1 - \alpha$ according to classical results about tolerance regions (Krishnamoorthy and Mathew, 2009), see also Lemma 1 in Romano et al. (2019).

C.5 Proof of Proposition A9

Proof To prove (24), note that $V = \{a_{j_1}, \dots, a_{j_k}\}$ if and only if there is a k -composition $c = (c_1, \dots, c_k)$ of M such that, for all $l \in [k]$, the sequence $(Z_{m+1}, \dots, Z_{m+M}) = (a_{t_1}, \dots, a_{t_M})$ contains exactly c_l values of a_{j_l} . For a given k -composition $c = (c_1, \dots, c_k)$, there are $\binom{M}{c_1 c_2 \dots c_k}$ indices $t_1, t_2, \dots, t_M \in \mathbb{N}$ such that for all $l \in [k]$, exactly c_l of them are equal to j_l . The probability that $(Z_{m+1}, \dots, Z_{m+M})$ equals any one of them is $p_{j_1}^{c_1} \dots p_{j_k}^{c_k}$, showing (24).

To prove (25), note that, for any $S \subset \mathbb{N}$, any product arising from the expansion of $(\sum_{l \in S} p_l)^M$ has at least one and at most M distinct indices l . Collecting the products $p_{i_1} p_{i_2} \dots p_{i_M}$ by the number $d \in \{1, \dots, M\}$ of distinct indices among their factors, we find

$$\left(\sum_{l \in S} p_l \right)^M = \sum_{d=1}^M \sum_{\{l_1, \dots, l_d\} \subset S, l_i \neq l_j \text{ for } i \neq j} \sum_{c \in C_{M,d}} \binom{M}{c_1 c_2 \dots c_d} p_{l_1}^{c_1} \dots p_{l_d}^{c_d}.$$

Now fix any $\{l_1, \dots, l_d\} \subset \{j_1, \dots, j_k\}$, and any $c \in C_{M,d}$. Using the previous formula for each S on the right hand side of (25), the total coefficient of $p_{l_1}^{c_1} \dots p_{l_d}^{c_d}$ is the following sum over subsets S

$$\binom{M}{c_1 c_2 \dots c_d} \sum_{S \subset \{j_1, \dots, j_k\}} (-1)^{k+|S|} I(\{l_1, \dots, l_d\} \subset S).$$

Writing the indicator $I(\{l_1, \dots, l_d\} \subset S)$ inside the summation constraint, and factoring out $(-1)^k$, this equals

$$(-1)^k \binom{M}{c_1 c_2 \dots c_d} \sum_{\{l_1, \dots, l_d\} \subset S \subset \{j_1, \dots, j_k\}} (-1)^{|S|}.$$

Now, if $\{l_1, \dots, l_d\} = \{j_1, \dots, j_k\}$, the above summation (after the pre-factor) has only one term— $S = \{j_1, \dots, j_k\}$ —and equals $(-1)^{|S|} = (-1)^k$.

Otherwise, the above summation contains $2^{k-d} > 1$ terms. We now construct a pairing of the sets S that index of the summation, such that each pair (S_1, S_2) contains an odd and even sized set. There must be an index j_a , $a \in [k]$, such that $j_a \notin \{l_1, \dots, l_d\}$. Suppose without loss of generality that we have $j_k \notin \{l_1, \dots, l_d\}$ (otherwise rename the indices j_a and j_k).

Then, for any set S_1 such that $\{l_1, \dots, l_d\} \subset S_1 \subset \{j_1, \dots, j_k\}$ that does not contain j_k , there is a corresponding set $S_2 = S_1 \cup \{j_k\}$ such that $\{l_1, \dots, l_d\} \subset S_2 \subset \{j_1, \dots, j_k\}$. Moreover, all sets S such that $\{l_1, \dots, l_d\} \subset S \subset \{j_1, \dots, j_k\}$ fall into exactly one such pair. Further, in each pair, there is one set of an odd size and one set of an even size.

Thus, in each pair, we have

$$(-1)^{|S_1|} + (-1)^{|S_2|} = 0,$$

Therefore, when $\{l_1, \dots, l_d\} \neq \{j_1, \dots, j_k\}$

$$\sum_{\{j_1, \dots, j_d\} \subset S \subset \{i_1, \dots, i_k\}} (-1)^{|S|} = 0.$$

Hence, the coefficient of $p_{j_1}^{c_1} \cdots p_{l_d}^{c_d}$ in the expression on the right hand side of (25) is nonzero only when $\{l_1, \dots, l_d\} = \{j_1, \dots, j_k\}$, in which case it equals

$$(-1)^{2k} \binom{M}{c_1 c_2 \dots c_d} = \binom{M}{c_1 c_2 \dots c_d}.$$

This shows that (24) and (25) coincide, completing the proof. ■

C.6 Proof of Proposition 4

Proof The formula in (17) follows directly from Equation (24) in Proposition A9, because for a set V of size k , the probability of any element being the selected unique ζ equals $1/k$. Next, $U_Z^{[1]} = P_Z$ by definition. In addition,

$$\begin{aligned} U_Z^{[2]}(\zeta = a_{j_1}) &= p_{j_1}^2 + \frac{1}{2} \sum_{J=\{j_1, j_2\} \subset \mathbb{N}^2, |J|=2} \sum_{c \in C_{2,2}} \binom{2}{c_1 c_2} p_{j_1}^{c_1} p_{j_2}^{c_2} \\ &= p_{j_1}^2 + \frac{1}{2} \sum_{j_2 \in \mathbb{N} \setminus \{j_1\}} 2p_{j_1} p_{j_2} = p_{j_1}^2 + p_{j_1}(1 - p_{j_1}) = p_{j_1}. \end{aligned}$$

This shows that $U_Z^{[2]} = P_Z$. Finally,

$$\begin{aligned} U_Z^{[3]}(\zeta = a_{j_1}) &= p_{j_1}^3 + \frac{1}{2} \sum_{J=\{j_1, j_2\} \subset \mathbb{N}^2, |J|=2} \sum_{c \in C_{3,2}} \binom{3}{c_1 c_2} p_{j_1}^{c_1} p_{j_2}^{c_2} + \frac{1}{3} \binom{3}{1 \ 1 \ 1} \sum_{J=\{j_1, j_2, j_3\} \subset \mathbb{N}^3, |J|=3} p_{j_1} p_{j_2} p_{j_3} \\ &= p_{j_1}^3 + \frac{1}{2} \sum_{J=\{j_1, j_2\} \subset \mathbb{N}^2, |J|=2} \sum_{c \in C_{3,2}} \binom{3}{c_1 c_2} p_{j_1}^{c_1} p_{j_2}^{c_2} + 2 \sum_{J=\{j_1, j_2, j_3\} \subset \mathbb{N}^3, |J|=3} p_{j_1} p_{j_2} p_{j_3}. \end{aligned}$$

This further equals

$$\begin{aligned} &p_{j_1}^3 + \frac{3}{2} \sum_{j_2 \in \mathbb{N} \setminus \{j_1\}} (p_{j_1}^2 p_{j_2} + p_{j_1} p_{j_2}^2) + 2p_{j_1} \sum_{\{j_2, j_3\} \subset (\mathbb{N} \setminus \{j_1\})^2, |J|=2} p_{j_2} p_{j_3} \\ &= p_{j_1}^3 + \frac{3}{2} p_{j_1}^2 (1 - p_{j_1}) + p_{j_1} \left(\frac{3}{2} \sum_{j_2 \in \mathbb{N} \setminus \{j_1\}} p_{j_2}^2 + 2 \sum_{\{j_2, j_3\} \subset (\mathbb{N} \setminus \{j_1\})^2, |J|=2} p_{j_2} p_{j_3} \right). \end{aligned}$$

By expanding the square in $(1 - p_{j_1})^2 = (\sum_{j_2 \in \mathbb{N} \setminus \{j_1\}} p_{j_2})^2$, this further equals

$$\begin{aligned} & \frac{p_{j_1}^2 (3 - p_{j_1})}{2} + p_{j_1} \left(\frac{3}{2} \left[(1 - p_{j_1})^2 - \sum_{\{j_2, j_3\} \subset (\mathbb{N} \setminus \{j_1\})^2, |J|=2} p_{j_2} p_{j_3} \right] \right. \\ & \quad \left. + 2 \sum_{\{j_2, j_3\} \subset (\mathbb{N} \setminus \{j_1\})^2, |J|=2} p_{j_2} p_{j_3} \right) \\ & = \frac{p_{j_1} (2p_{j_1}^2 - 3p_{j_1} + 3)}{2} + \frac{p_{j_1}}{2} \sum_{\{j_2, j_3\} \subset (\mathbb{N} \setminus \{j_1\})^2, |J|=2} p_{j_2} p_{j_3}. \end{aligned}$$

This finishes the proof. ■

C.7 Proof of Proposition 5

Proof Let the two objects be denoted by a_1 and a_2 . Then, one can verify using (25) in Proposition A9 and (17) in Proposition 4 that, for $j = 1, 2$,

$$U_Z^{[M]}(\zeta = a_j) = \frac{1 + p_j^M - (1 - p_j)^M}{2}. \quad (26)$$

Therefore,

$$\Delta(M, M'; 2) = \frac{1}{2} \sup_{p \in [0, 1]} \left| p^M - (1 - p)^M - \left[p^{M'} - (1 - p)^{M'} \right] \right|.$$

Let $\delta = (1 - p)/p \geq 0$, so that $p = 1/(1 + \delta)$, and suppose without loss of generality that $\delta \leq 1$; otherwise, change variables to $1 - p \leftarrow p$. Then, the term inside the absolute value above can be written as

$$A(\delta) = \frac{1 - \delta^{M'}}{(1 + \delta)^{M'}} - \frac{1 - \delta^M}{(1 + \delta)^M} \geq 0. \quad (27)$$

Now, denoting, for $c \geq 1$, $g(\delta, c) = \frac{1 - \delta^c}{(1 + \delta)^c}$, we have

$$\begin{aligned} \frac{\partial g(\delta, c)}{\partial \delta} &= \frac{-c\delta^{c-1}(1 + \delta)^c - (1 - \delta^c) \cdot c(1 + \delta)^{c-1}}{(1 + \delta)^{2c}} \\ &= -c \frac{\delta^{c-1}(1 + \delta) + (1 - \delta^c)}{(1 + \delta)^{c+1}} = -c \frac{1 + \delta^{c-1}}{(1 + \delta)^{c+1}}. \end{aligned}$$

Hence,

$$A'(\delta) = -M' \frac{1 + \delta^{M'-1}}{(1 + \delta)^{M'+1}} + M \frac{1 + \delta^{M-1}}{(1 + \delta)^{M+1}}.$$

Thus, $A'(\delta) \geq 0$ is equivalent to

$$\frac{1 + \delta^{M-1}}{1 + \delta^{M'-1}} \geq \frac{M'}{M} (1 + \delta)^{M-M'},$$

or, with the function h defined as in (20), to $h(\delta) \geq \ln(M'/M)$. Now,

$$h'(\delta) = \frac{(M-1)\delta^{M-2}}{1+\delta^{M-1}} - \frac{(M'-1)\delta^{M'-2}}{1+\delta^{M'-1}} - \frac{M-M'}{1+\delta}.$$

We claim that $h'(\delta) < 0$ for all $\delta \in [0, 1)$. Indeed, this is equivalent to the function

$$\tilde{\psi}(M) = \frac{M}{1+\delta} - \frac{(M-1)\delta^{M-2}}{1+\delta^{M-1}}$$

being increasing in M , for all $M \geq 2$. Denote $x = M - 1 \geq 1$, $\psi(x) = \delta \cdot \tilde{\psi}(x + 1)$, and $a = 1/\delta \geq 1$. Then,

$$\psi(x) = \frac{x+1}{1+a} - \frac{x}{1+a^x}$$

and

$$\psi'(x) = \frac{1}{1+a} - \frac{1+a^x - xa^x \ln a}{(1+a^x)^2}.$$

Hence, $\psi'(x) > 0$ is equivalent to

$$(1+a)(1+a^x - xa^x \ln a) < (1+a^x)^2.$$

Now, since $a \geq 1$ and $x \geq 1$, we have $1+a \leq 1+a^x$ and $xa^x \ln a \geq 0$. Equality happens in both equations if and only if $x = 1$ and $a = 1$. This corresponds to $M = 2$ and $\delta = 1$. Thus, the above inequality holds for all $\delta \in [0, 1)$. This shows that h is decreasing for $\delta \in [0, 1)$. Since $h(0) = 0$ and $h(1) = M' - M \leq \ln(M'/M)$, and as h is continuous on $[0, 1]$, there is a unique solution $\delta_* \in [0, 1]$ to $h(\delta_*) = \ln(M'/M)$. This proves the first claim. Based on our analysis, it follows that A is maximized over $[0, 1]$ at δ_* . This finishes the proof. \blacksquare

C.8 Proof of Corollary 6

Proof Recalling the function h from (20), the equation for $\delta \in [0, 1]$ from Proposition 5 is

$$\frac{M}{M'}(\delta^{M-1} + 1) = (1 + \delta^{M'-1})(1 + \delta)^{M-M'}.$$

For $M = aM'$,

$$a(\delta^{aM'-1} + 1) = (1 + \delta^{M'-1})(1 + \delta)^{(a-1)M'}. \quad (28)$$

Hence, as $a \geq 1$, $2a \geq (1 + \delta)^{(a-1)M'}$, and thus

$$1 + \delta \leq (2a)^{1/[(a-1)M']} \leq 1 + \frac{\ln(2a)}{(a-1)M'}.$$

Hence, $\delta \leq \frac{\ln(2a)}{(a-1)M'}$. For $M' \geq 2\ln(2a)/(a-1)$, we thus find $\delta \leq 1/2$. Using this in (28), we obtain

$$\frac{a}{1 + 2^{-(M'-1)}} \leq (1 + \delta)^{(a-1)M'} \leq a \left(1 + 2^{-(aM'-1)}\right).$$

Given two sequences $(A_{M'})_{M' \geq 1}$, $(B_{M'})_{M' \geq 1}$, we will write $A_{M'} \sim B_{M'}$, if as $M' \rightarrow \infty$, $|A_{M'}/B_{M'} - 1| = O(1/M')$. Denoting by δ_* the unique solution of (28), from the above display, we find $(1 + \delta_*)^{(a-1)M'} \sim a$. Therefore, $(1 + \delta_*)^{M'} \sim a^{1/(a-1)}$ and $(1 + \delta_*)^{aM'} \sim a^{a/(a-1)}$. Hence, with A from (27),

$$A(\delta_*) = \frac{1 - \delta_*^{M'}}{(1 + \delta_*)^{M'}} - \frac{1 - \delta_*^M}{(1 + \delta_*)^{aM'}} \sim a^{-1/(a-1)} - a^{-a/(a-1)} = a^{-1/(a-1)}(1 - 1/a).$$

Finally, $\Delta(M, M'; 2) \sim A(\delta_*)$ from the proof of Proposition 5, completing this proof. \blacksquare

C.9 Proof of Theorem 7

Proof This follows immediately by combining Corollary 6 with (19) and Theorem 3. \blacksquare

C.10 Proof of Theorem 8

Proof First, we aim to show that, for $p_j \neq p'_j$,

$$|U_Z^{[M]}(\{a_j\}) - U_{Z'}^{[M]}(\{a_j\})| < |p_j - p'_j|. \quad (29)$$

For simplicity of notation, define $p := p_i$ and $q := p'_i$. Define also $d : [0, 1] \rightarrow \mathbb{R}$ as $d(p) = [p^M - (1-p)^M]/2$, for all $p \in [0, 1]$. It follows from (26) that we need to show

$$|d(p) - d(q)| < |p - q|.$$

Suppose without loss of generality that $p < q$. By the mean value theorem applied to d , there exists a $\omega \in [p, q]$, such that $d(p) - d(q) = d'(\omega)(p - q)$. Therefore, it suffices to show that $|d'(\omega)| < 1$ for $\omega \in (c, 1 - c)$. Now, $d'(\omega) = M[\omega^{M-1} + (1-\omega)^{M-1}]/2$. We note here that $d'(0) = M/2 > 1$, $d'(1/2) = M/2^{M-1} < 1$ (as $M \geq 3$), and d' is strictly decreasing as a function of ω for $\omega \in [0, 1/2]$. Therefore, the equation $d'(c) = 1$ has a unique solution over $c \in [0, 1/2]$. This shows that c in (21) is well defined.

Moreover, because d' is strictly decreasing between $[0, 1/2]$, it follows that d' is maximized within the interval $[c, 1 - c]$ at c and (by symmetry) at $1 - c$. Therefore, $|d'(\omega)| < 1$ for $\omega \in (c, 1 - c)$, and (29) follows.

Let $TV(\cdot, \cdot)$ be the total variation distance. Then, for all $P_Z, P_{Z'} \in \mathcal{S}_c$, with $P_Z \neq P_{Z'}$,

$$TV(U_Z^{[M]}, U_{Z'}^{[M]}) < TV(P_Z, P_{Z'}). \quad (30)$$

Following (19), define $e_U(Z^*) = \mathbb{P}_{\tilde{Z}_{1:G} \sim (U_Z^{[M]})^{|G|}}[\mathcal{E}]$ and $e(Z^*) = \mathbb{P}_{\tilde{Z}_{1:G} \sim P_Z^{|G|}}[\mathcal{E}]$. Let A_U, A be the sets of functions over which e_U, e can range, respectively. We need to show that

$$\sup_{e_U \in A_U} \left| \mathbb{E}_{Z^* \sim U_Z^{[M]}} e_U(Z^*) - \mathbb{E}_{Z^* \sim U_{Z'}^{[M]}} e_U(Z^*) \right| < \sup_{e \in A} \left| \mathbb{E}_{Z^* \sim P_Z} e(Z^*) - \mathbb{E}_{Z^* \sim P_{Z'}} e(Z^*) \right|.$$

Because $\mathcal{E} \subset \{a_1, a_2\}^{|G|+1}$ is arbitrary, the possible values of e_U include zero and unity, for any value $Z^* = z$. Hence, the above inequality is equivalent to (30), completing the proof. \blacksquare

D. Additional experiments with two-sided confidence intervals

This section describes additional experiments with synthetic data similar to those described in Figures 1 (Zipf distribution) and A10 (Pitman-Yor process prior), constructing two-sided instead of one-sided confidence intervals. For simplicity, we focus on one-sided 95% conformalized bootstrap confidence intervals based on the simpler Bonferroni approach described in Section A.3.2. The performance of these intervals is compared to those of one and two-sided standard bootstrap confidence intervals obtained with the method of Ting (2018).

Figure A28 reports on results based on data generated from a Zipf distribution and sketched with the CMS-CU, similarly to Figure 1. Here, all methods achieve the desired 95% marginal coverage level, but the conformal confidence intervals are shorter when the Zipf tail parameter a is larger and hash collisions become rarer, consistently with Figure 1. It is interesting to note that the two-sided conformal confidence intervals are much narrower than their one-sided counterparts when a is small and hash collisions are very common, but this is not true if a is large. The latter is likely a limitation of the specific construction we have adopted, described in Section A.3.2, which may be too conservative in some cases due to the Bonferroni correction. A suitable implementation of the more sophisticated conditional histogram (Sesia and Romano, 2021) approach described in Section A.3.1 should be expected to produce two-sided intervals that are always narrower than their one-sided counterparts. Figure A29 reports on results similar to those in Figure A28, with the only difference that now the data are sketched with the vanilla CMS instead of the CMS-CU.

Figure A30 reports on results based on data generated from a Pitman-Yor process prior and sketched with the CMS-CU, similarly to Figure A10. Here, all methods achieve the desired 95% marginal coverage level, and two-sided intervals are generally much shorter than their one-sided counterparts. Across all values of σ , the conformal confidence intervals tend to be shorter than the bootstrap intervals, although this difference becomes very small in the case of two-sided intervals for large values of σ . Finally, Figure A31 reports on results similar to those in Figure A30, with the only difference that now the data are sketched with the vanilla CMS instead of the CMS-CU.

E. Supplementary figures and tables

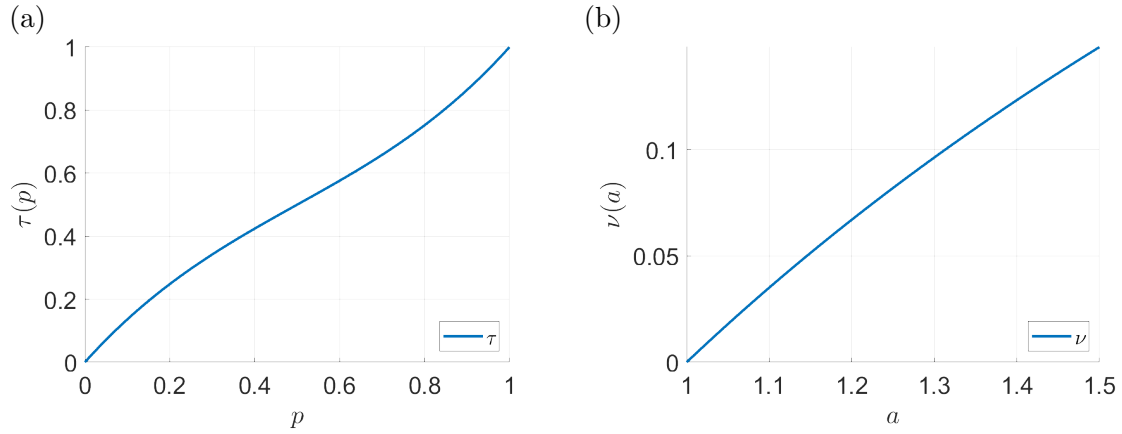


Figure A7: (a) Plot of the function τ defined in (18). (b) Plot of the function $a \mapsto \nu(a) := a^{-1/(a-1)}(1 - 1/a)$ defined in Corollary 6.

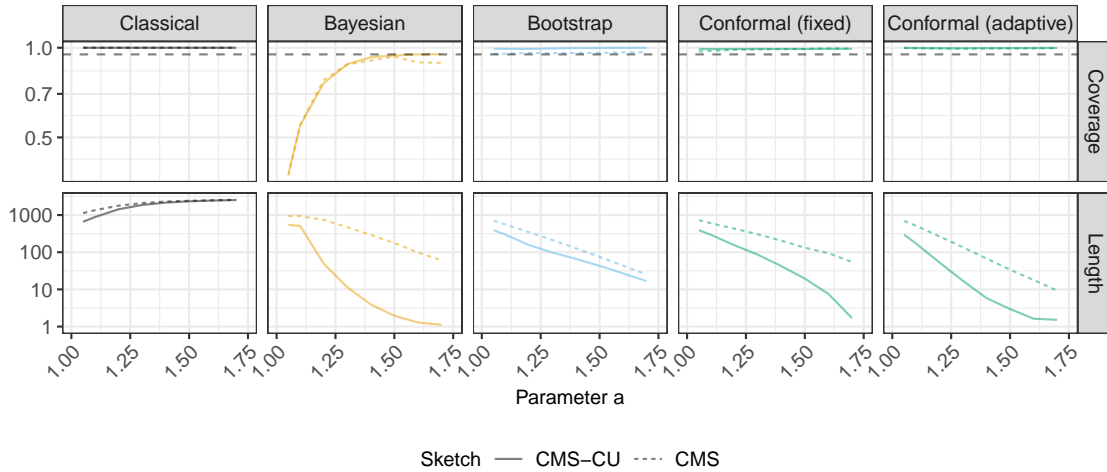


Figure A8: Performance of 95% confidence intervals for random queries, based on synthetic data from a Zipf distribution. The data are sketched with either the vanilla CMS or the CMS-CU. The results are shown as a function of the Zipf tail parameter a . Other details are as in Figure 1.

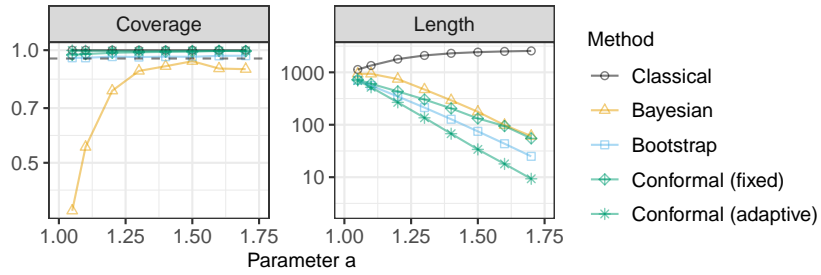


Figure A9: Performance of 95% confidence intervals for random queries, based on synthetic data from a Zipf distribution, sketched with the vanilla CMS. The results are shown as a function of the Zipf tail parameter a . Other details are as in Figure 1.

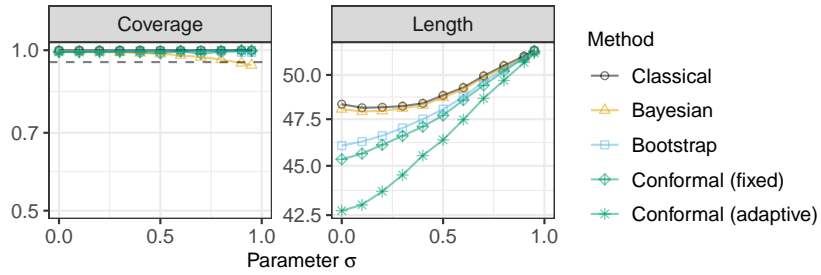


Figure A10: Empirical coverage and length of 95% confidence intervals for random queries on synthetic data from the predictive distribution of a Pitman-Yor process. The data are sketched with the CMS-CU. The results are shown as a function of the Pitman-Yor process parameter σ . Other details are as in Figure 1.

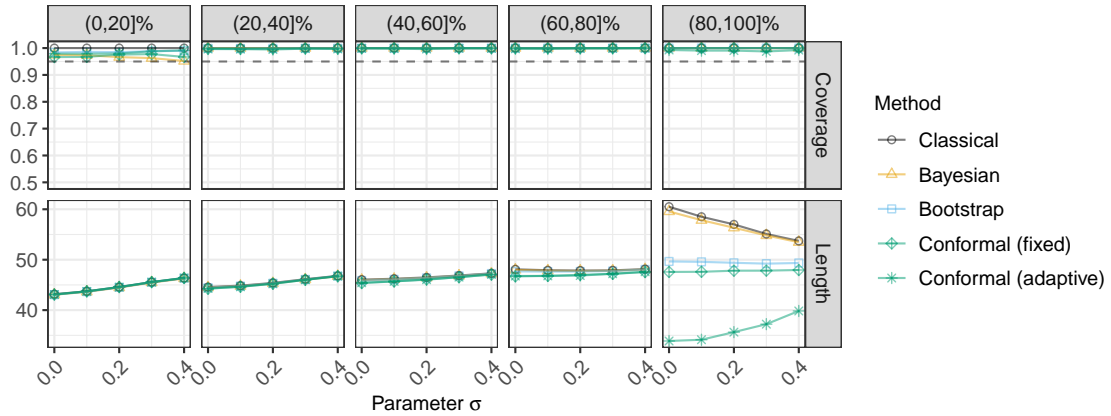


Figure A11: Performance of confidence intervals for random queries on synthetic data from the predictive distribution of a Pitman-Yor process. The results are stratified by the quintile of the true query frequency. Other details are as in Figure A10.

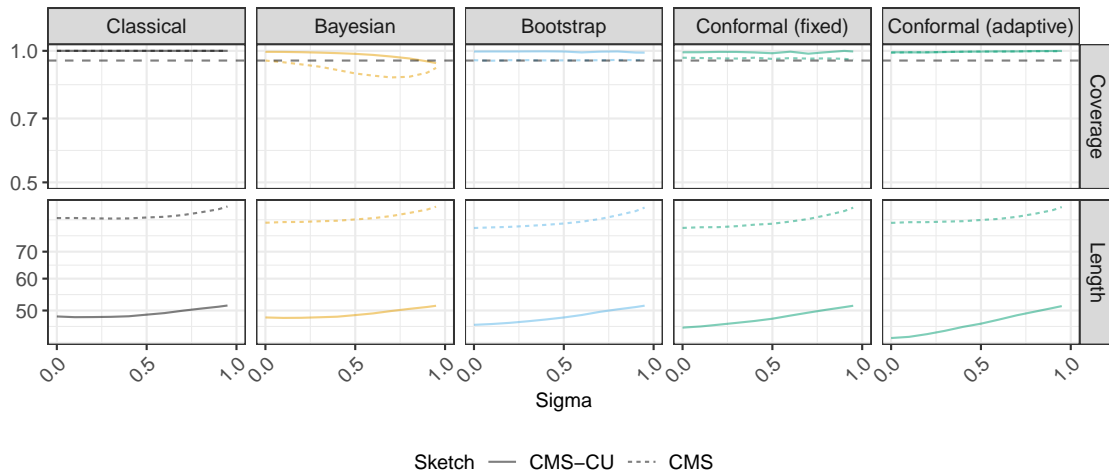


Figure A12: Performance of 95% confidence intervals for random queries, based on synthetic data from the predictive distribution of a Pitman-Yor process and sketched with either the vanilla CMS or the CMS-CU. The results are shown as a function of the Pitman-Yor process parameter σ . Other details are as in Figure A10.

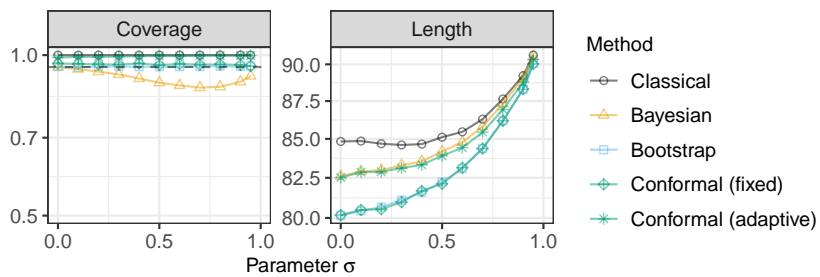


Figure A13: Performance of 95% confidence intervals for random queries, based on synthetic data from the predictive distribution of a Pitman-Yor process and sketched with the vanilla CMS. The results are shown as a function of the Pitman-Yor process parameter σ . Other details are as in Figure A10.

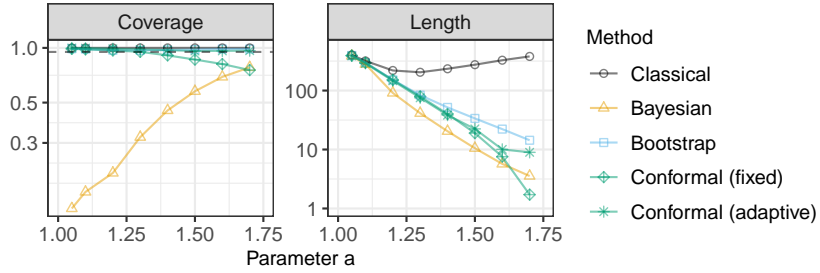


Figure A14: Performance of confidence intervals for random queries on synthetic Zipf data, keeping only unique queries. The coverage is the empirical proportion of unique queries whose frequency is covered by the output confidence intervals. The conformal confidence intervals are computed by applying Algorithm 3 with $L = 5$ frequency bins. Other details are as in Figure 1.

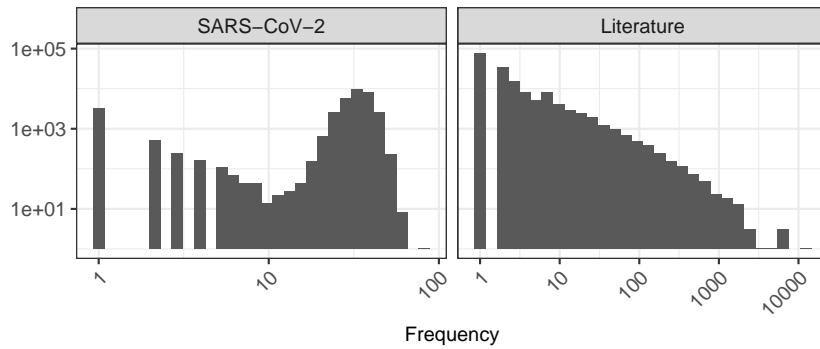


Figure A15: True frequency distribution of unique objects in two empirical data sets. Left: sequenced SARS-CoV-2 DNA 16-mers. Right: English 2-grams in a corpus of classic English literature.

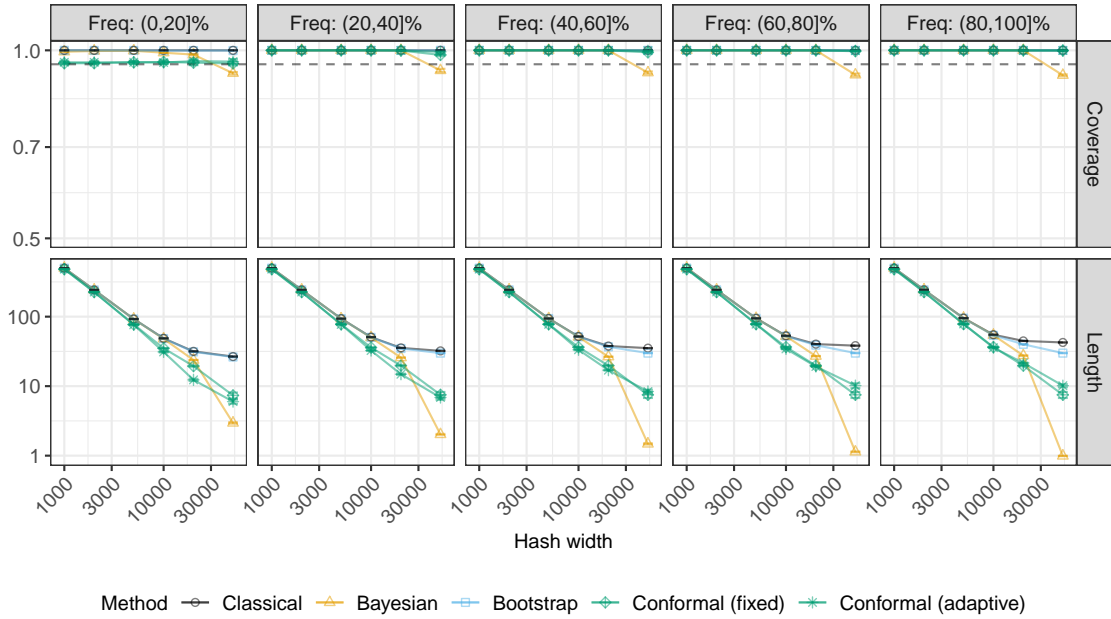


Figure A16: Performance of 95% confidence intervals for random queries on SARS-CoV-2 sequence data sketched with the CMS-CU. The results are shown as a function of the hash width and stratified by the quintile of the true query frequency. Other details are as in Figure 5.

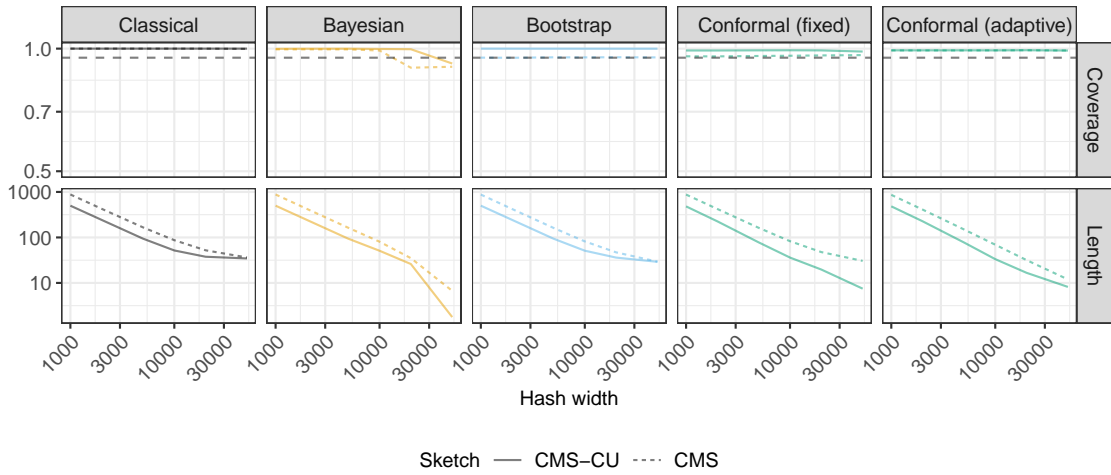


Figure A17: Performance of 95% confidence intervals for random queries on SARS-CoV-2 sequence data. The data are sketched with either the vanilla CMS or the CMS-CU. The results are shown as a function of the hash width. Other details are as in Figure 5.

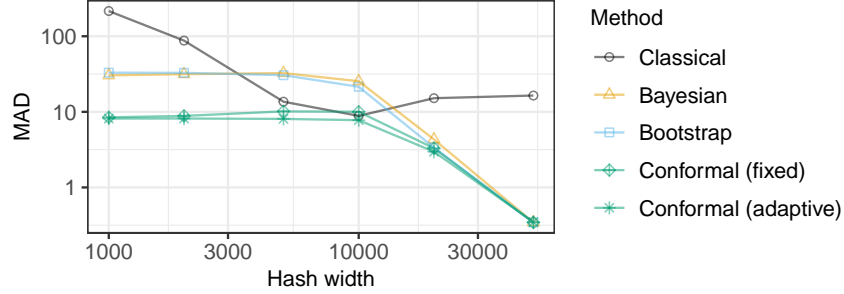


Figure A18: Median absolute deviation of point estimates for random queries on SARS-CoV-2 sequence data sketched with the CMS-CU. The results are shown as a function of the hash width. Other details are as in Figure 5.

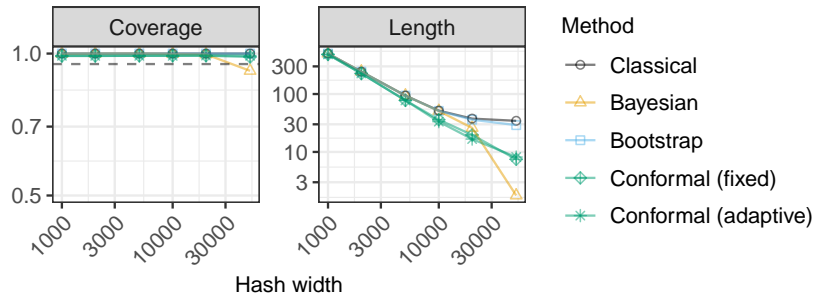


Figure A19: Performance of 95% confidence intervals for random queries, on a sketched data set of 2-grams in classic English literature, keeping only unique queries. The coverage is the empirical proportion of unique queries whose frequency is covered by the output confidence intervals. The conformal confidence intervals are computed by applying Algorithm 3 with $L = 5$ frequency bins. The data are sketched with the CMS-CU. Other details are as in Figure 5.

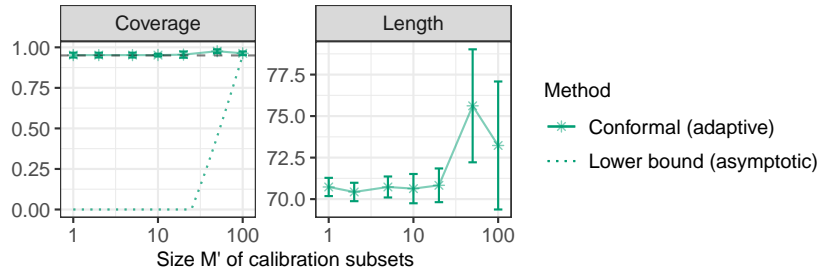


Figure A20: Performance on sketched SARS-CoV-2 data of confidence intervals for unique queries in a test set of size $M = 100$, as a function of the parameter M' of Algorithm 4 for constructing conformal confidence intervals satisfying (16). The hash width is $w = 5000$. Other details are as in Figure 5.

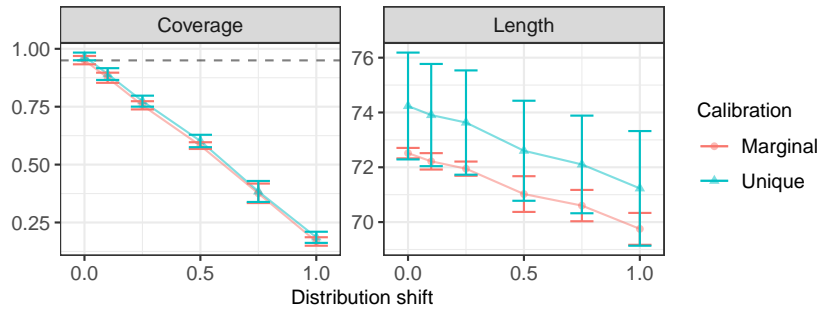


Figure A21: Performance on sketched SARS-CoV-2 data of conformal confidence intervals with marginal (Algorithm 2) or unique-query (Algorithm 4) coverage in a test set of size 100 with varying degrees of distribution shift. Other details are as in Figure 5.

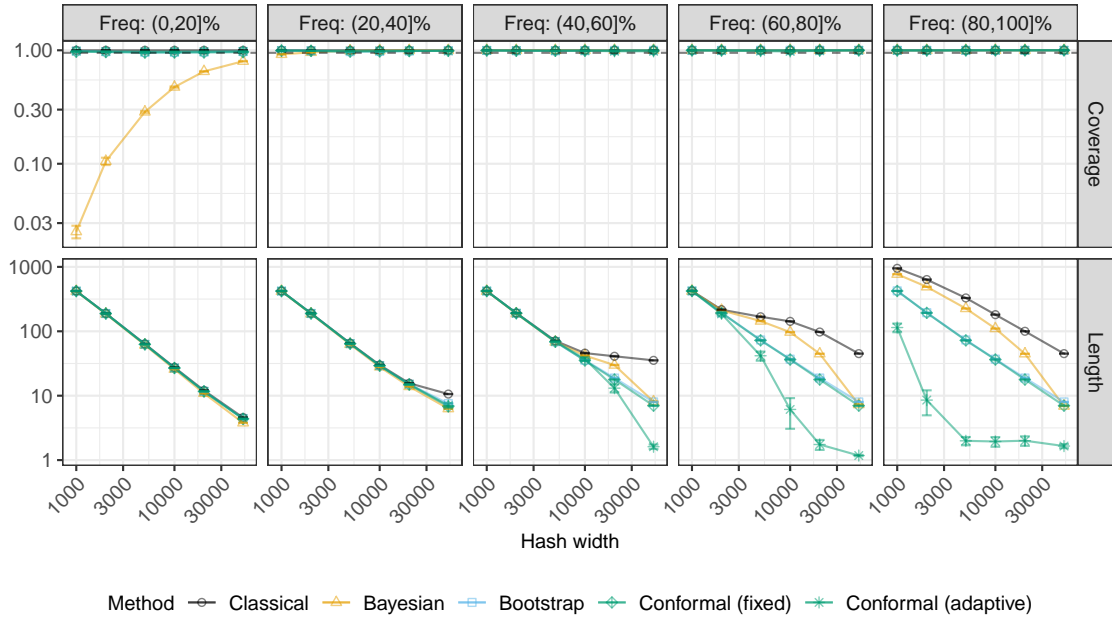


Figure A22: Performance of 95% confidence intervals for random queries on a data set of 2-grams in classic English literature, sketched with the CMS-CU. The results are shown as a function of the hash width and stratified by the quintile of the true query frequency. Other details are as in Figure 6.

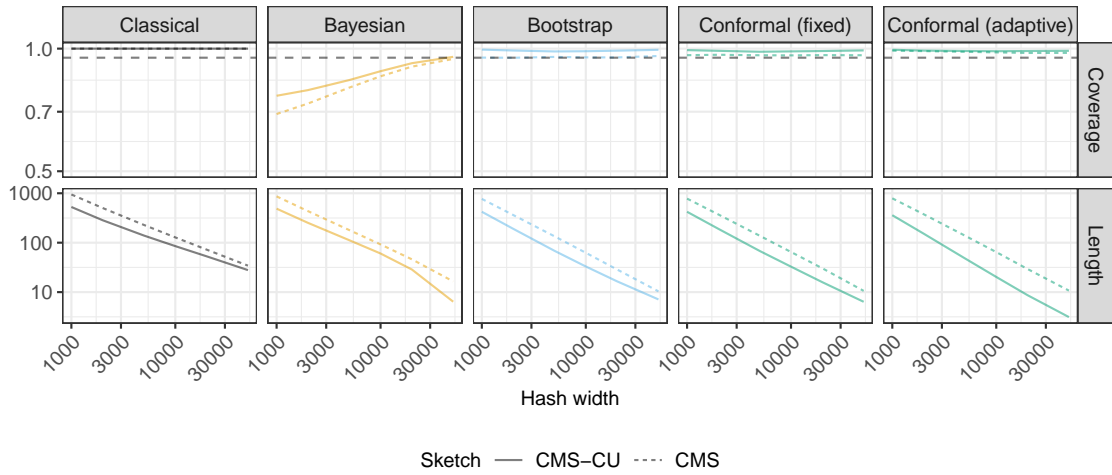


Figure A23: Performance of 95% confidence intervals for random queries on a data set of 2-grams in classic English literature. The data are sketched with either the vanilla CMS or the CMS-CU. The results are shown as a function of the hash width. Other details are as in Figure 6.

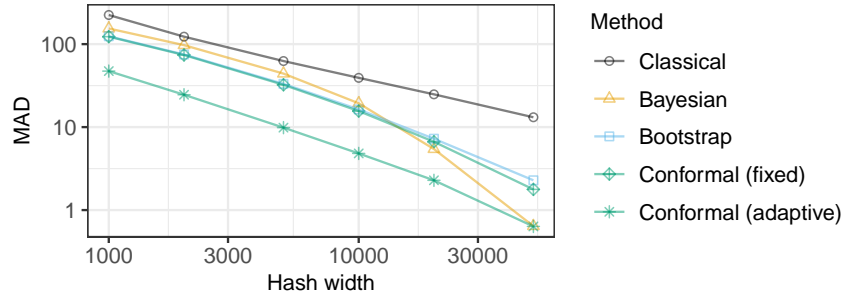


Figure A24: Median absolute deviation of point estimates for random queries on a data set of 2-grams in classic English literature, sketched with the CMS-CU. The results are shown as a function of the hash width. Other details are as in Figure 6.

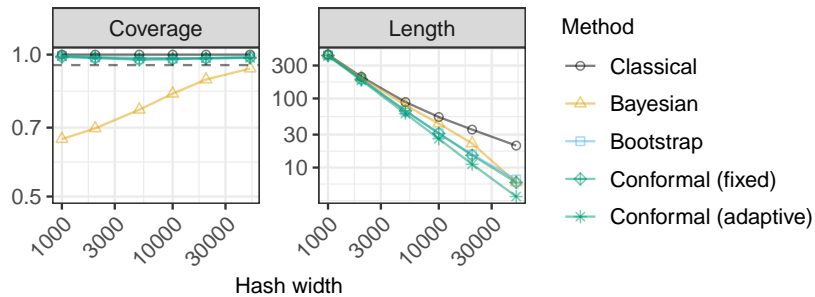


Figure A25: Performance of 95% confidence intervals for random queries, on a sketched data set of 2-grams in classic English literature, keeping only unique queries. The coverage is the empirical proportion of unique queries whose frequency is covered by the output confidence intervals. The conformal confidence intervals are computed by applying Algorithm 3 with $L = 5$ frequency bins. Other details are as in Figure 6.

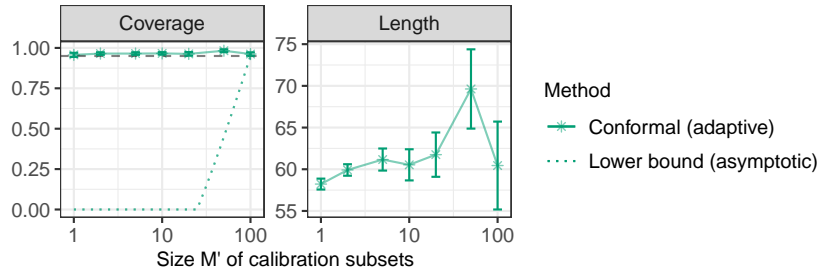


Figure A26: Performance on sketched English literature data of confidence intervals for unique queries in a test set of size $M = 100$, as a function of the parameter M' of Algorithm 4 for constructing conformal confidence intervals satisfying (16). The hash width is $w = 5000$. Other details are as in Figure 6.

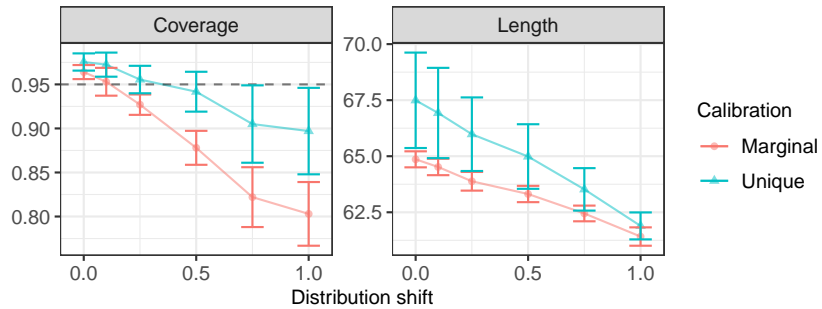


Figure A27: Performance on sketched English literature data of conformal confidence intervals with marginal (Algorithm 2) or unique-query (Algorithm 4) coverage in a test set of size 100 with varying degrees of distribution shift. Other details are as in Figure 6.

Table A1: True frequencies, deterministic upper bounds, and 95% lower bounds for 10 common (top) and 10 rare (bottom) random queries in two sketched data sets. Sketching with CMS-CU with $w = 50,000$. Lower bounds written in green are below the true frequency; those in red are above. For each query, the highest lowest bound below the true frequency is highlighted in bold.

Data	Frequency	Upper bound	95% Lower bound					
			Classical	Bayesian	Bootstrap	Conformal		
						Fixed	Adaptive	
SARS-CoV-2								
AATTATTATAAGAAAG	81	81	26	81	52	50	36	
TCAGACAACACTACTATT	76	76	21	55	47	45	32	
AAAGTTGATGGTGTG	73	73	18	59	44	42	31	
CAATTATTATAAGAAA	63	63	8	48	34	32	26	
ATCAGACAACACTACTAT	60	60	5	44	31	29	26	
ACCTTTGACAATCTTA	55	55	0	52	26	24	27	
ATTTGAAGTCACCTAA	55	55	0	55	26	24	27	
CATGCAAATTACATAT	54	54	0	54	25	23	26	
GAATTTACAGTATTC	54	54	0	54	25	23	27	
TTTGTAGAAAACCCAG	53	53	0	53	24	22	27	
AGTTGCAGAGTGGTTT	24	24	0	13	0	0	20	
TCTTCACAATTGGAAC	24	24	0	12	0	1	20	
TTCTGCTCGCATAGTG	24	24	0	12	0	0	20	
CTACTTTAGATTCGAA	23	23	0	11	0	0	19	
GCTGGTGTCTCTATCT	23	23	0	23	0	1	19	
TTCTAAGAAGCCTCGG	23	24	0	14	0	0	20	
GGGCTGTTGTTCTTGT	22	24	0	12	0	0	20	
ACGTTTCGTGTTGTTTT	20	20	0	20	0	0	16	
GAAGTCTTTGAATGTG	20	20	0	20	0	0	16	
CAAACCTGGTAATTTTT	3	3	0	3	0	0	0	
Literature								
of the	12565	12568	12513	12544	12557	12556	12562	
in the	6188	6190	6135	6169	6179	6179	6180	
and the	6173	6175	6120	6151	6164	6164	6165	
the of	6015	6017	5962	5990	6006	6006	6007	
the lord	4186	4195	4140	4165	4184	4184	4184	
to the	3465	3467	3412	3445	3456	3456	3463	
the and	2250	2251	2196	2227	2240	2240	2248	
all the	2226	2230	2175	2207	2219	2219	2224	
and he	2169	2173	2118	2153	2162	2162	2167	
to be	2062	2064	2009	2043	2053	2053	2060	
man on	22	29	0	10	18	18	18	
their hand	22	24	0	9	13	13	0	
no need	20	28	0	9	17	17	16	
and brother	12	14	0	2	3	3	0	
miss would	10	13	0	3	2	2	0	
i please	8	12	0	3	1	1	1	
also how	3	13	0	2	2	2	0	
in under	3	9	0	2	0	0	0	
ten old	3	6	0	1	0	0	0	
fault he	1	9	0	1	0	0	0	

Table A2: True frequencies, upper and lower bounds for 10 common (top) and 10 rare (bottom) random queries in two sketched data sets. Hash width $w = 50,000$. Other details are as in Table A1.

Data	Frequency	Upper bound	95% Lower bound				
			Classical	Bayesian	Bootstrap	Conformal	
						Fixed	Adaptive
SARS-CoV-2							
AATTATTATAAGAAAG	81	209	0	4	0	0	18
TCAGACAACTACTATT	76	213	0	8	0	0	18
AAAGTTGATGGTGTG	73	130	0	2	0	1	18
CAATTATTATAAGAAA	63	233	0	4	11	6	19
ATCAGACAACTACTAT	60	179	0	2	0	0	18
ACCTTTGACAATCTTA	55	292	0	15	70	67	22
ATTTGAAGTCACCTAA	55	258	0	11	36	31	20
CATGCAAATTACATAT	54	204	0	3	0	0	18
GAATTTACAGTATTC	54	260	0	12	38	35	22
TTTGTAGAAAACCCAG	53	246	0	7	24	18	20
ATGCTGCAATCGTGCT	24	139	0	2	0	0	17
ATTCCTAATATTACA	24	92	0	1	0	0	17
CTCTATCATTATTGGT	24	121	0	1	0	0	17
TGTTTTATTCTCTACA	24	199	0	3	0	1	19
CAGTACATCGATATCG	23	119	0	2	0	0	17
TAATGGTGACTIONTTT	23	92	0	1	0	0	17
CAACCATAAAACCAGT	22	105	0	1	0	0	17
AGTTATTTGACTCCTG	21	97	0	1	0	1	18
ATAAAGGAGTTGCACC	19	218	0	5	0	0	18
Literature							
of the	12565	12630	12086	12325	12463	12454	12563
in the	6188	6242	5698	5906	6075	6067	6096
and the	6173	6314	5770	5972	6147	6139	6169
the of	6015	6162	5618	5834	5995	5985	6014
the lord	4186	4289	3745	3975	4122	4114	4185
to the	3465	3558	3014	3217	3391	3380	3464
the and	2250	2413	1869	2081	2246	2237	2249
all the	2226	2346	1802	1993	2179	2170	2225
and he	2169	2293	1749	1937	2126	2117	2168
to be	2062	2121	1577	1770	1954	1945	2061
very for	15	59	0	2	0	0	0
and faithful	14	94	0	3	0	0	0
but found	9	74	0	2	0	0	0
my speech	6	98	0	3	0	0	0
of eight	5	66	0	2	0	0	0
and soul	4	140	0	6	0	0	0
her prow	3	79	0	2	0	0	0
usual as	2	56	0	2	0	0	0
a invitation	1	80	0	2	0	0	0
angular log	0	146	0	5	0	0	0

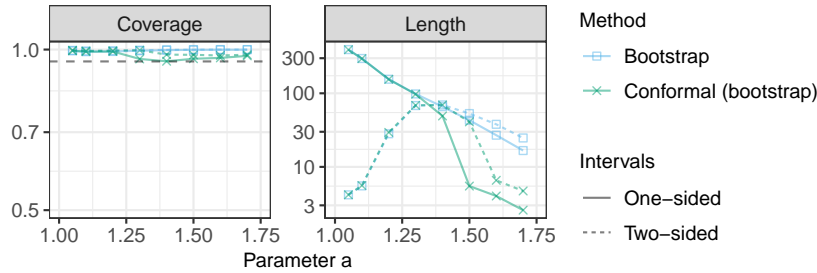


Figure A28: Performance of 95% one-sided and two-sided confidence intervals with data from a Zipf distribution, sketched with the CMS-CU. The results are shown as a function of the Zipf tail parameter a . Standard errors would be too small to be clearly visible in this figure, and are hence omitted. The two dashed curves for the two-sided intervals are nearly indistinguishable from one another for $a < 1.3$. Other details are as in Figure 1.

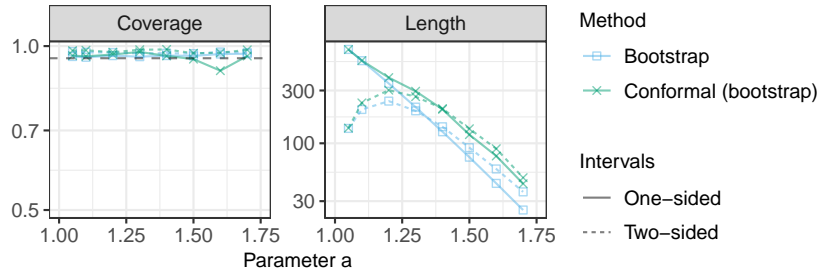


Figure A29: Performance of 95% one-sided and two-sided confidence intervals with data from a Zipf distribution, sketched with the vanilla CMS. The results are shown as a function of the Zipf tail parameter a . The two dashed curves for the two-sided intervals are nearly indistinguishable from one another for $a < 1.1$. Other details are as in Figure A28.

Figure A30 reports on results based on data generated from a Pitman-Yor process prior and sketched with the CMS-CU, similarly to Figure A10. As expected, the conformal confidence intervals are narrower than the bootstrap ones. Further, two-sided confidence intervals are much more efficient (narrower) compared to their one-sided counterparts, especially if the Pitman-Yor parameter σ is large and the number of hash collisions is high. Figure A31 reports on analogous results obtained with data sketched through the vanilla CMS instead of the CMS-CU.

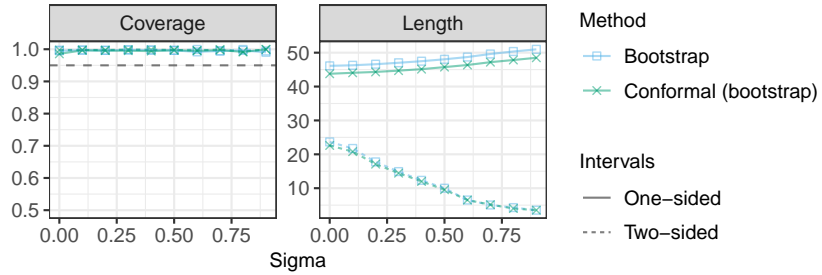


Figure A30: Performance of 95% one-sided and two-sided confidence intervals with data set sampled from the predictive distribution of a Pitman-Yor process and sketched with the CMS-CU. The results are shown as a function of the Pitman-Yor process parameter σ . The two dashed curves for the two-sided intervals are nearly indistinguishable from one another. Other details are as in Figure A10.

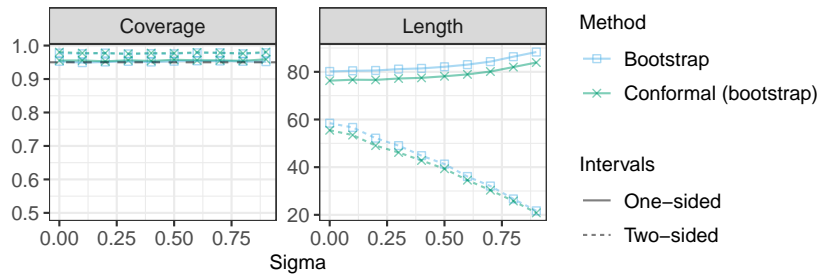


Figure A31: Performance of 95% one-sided and two-sided confidence intervals with data set sampled from the predictive distribution of a Pitman-Yor process and sketched with the vanilla CMS. The results are shown as a function of the Pitman-Yor process parameter σ . Other details are as in Figure A30.